Evaluation of the LSA-SAF gross primary production product derived from SEVIRI/MSG data (MGPP)

Martinez, B.

2020-01

Martinez , B , Gilabert , M A , Sanchez-Ruiz , S , Campos-Taberner , M , Garcia-Haro , F J , Bruemmer , C , Carrara , A , Feig , G , Gruenwald , T , Mammarella , I & Tagesson , T 2020 , ' Evaluation of the LSA-SAF gross primary production product derived from SEVIRI/MSG data (MGPP) ' , ISPRS Journal of Photogrammetry and Remote Sensing , vol. 159 , pp. 220-236 . https://doi.org/10.1016/j.isprsjprs.2019.11.010

http://hdl.handle.net/10138/314145
https://doi.org/10.1016/j.isprsjprs.2019.11.010

ISPRS Journal of Photogrammetry and Remote Sensing 159 (2020) 220–236

Contents lists available at ScienceDirect

ISPRS Journal of Photogrammetry and Remote Sensing

journal homepage: www.elsevier.com/locate/isprsjprs

Evaluation of the LSA-SAF gross primary production product derived from SEVIRI/MSG data (MGPP)

B. Martínez[a,*], M.A. Gilabert[a], S. Sánchez-Ruiz[a], M. Campos-Taberner[a], F.J. García-Haro[a], C. Brümmer[b], A. Carrara[c], G. Feig[d,e], T. Grünwald[f], I. Mammarella[g], T. Tagesson[h,i]

[a] Departament de Física de la Terra i Termodinàmica, Facultat de Física, Universitat de València, Burjassot, Spain
[b] Thünen Institute of Climate-Smart Agriculture, Braunschweig, Germany
[c] Fundación Centro de Estudios Ambientales del Mediterráneo (CEAM), Paterna, Spain
[d] Global Change and Ecosystems Dynamics, Natural Resources and Environment, Council for Scientific and Industrial Research (CSIR), Pretoria, South Africa
[e] Department of Geography, Geoinformatics and Meteorology, University of Pretoria, Pretoria, South Africa
[f] Technische Universität Dresden, Institute of Hydrology and Meteorology, Tharandt, Germany
[g] Institute for Atmospheric and Earth System Research/Physics, Faculty of Science, University of Helsinki, Helsinki, Finland
[h] Department of Physical Geography and Eosystem Sciences, Lund University, Lund, Sweden
[i] Department of Geosciences and Natural Resource Management (IGN), University of Copenhagen, Copenhagen, Denmark

ARTICLE INFO

Keywords:
GPP
SEVIRI/MSG
10-day
LSA SAF
Water stress
Light-use efficiency
MGPP

ABSTRACT

The objective of this study is to describe a completely new 10-day gross primary production (GPP) product (MGPP LSA-411) based on data from the geostationary SEVIRI/MSG satellite within the LSA SAF (Land Surface Analysis SAF) as part of the SAF (Satellite Application Facility) network of EUMETSAT.

The methodology relies on the Monteith approach. It considers that GPP is proportional to the absorbed photosynthetically active radiation APAR and the proportionality factor is known as the light use efficiency ε. A parameterization of this factor is proposed as the product of a ε_{max}, corresponding to the canopy functioning under optimal conditions, and a coefficient quantifying the reduction of photosynthesis as a consequence of water stress. A three years data record (2015–2017) was used in an assessment against site-level eddy covariance (EC) tower GPP estimates and against other Earth Observation (EO) based GPP products. The site-level comparison indicated that the MGPP product performed better than the other EO based GPP products with 48% of the observations being below the optimal accuracy (absolute error $<$ 1.0 g m^{-2} day^{-1}) and 75% of these data being below the user requirement threshold (absolute error $<$ 3.0 g m^{-2} day^{-1}). The largest discrepancies between the MGPP product and the other GPP products were found for forests whereas small differences were observed for the other land cover types. The integration of this GPP product with the ensemble of LSA-SAF MSG

Abbreviations: AET, actual evapotranspiration; APAR, absorbed photosynthetically active radiation; AVHRR, advanced very high resolution radiometer; BPLUT, biome property look up table; BRDF, bidirectional reflectance distribution function; CGLS, copernicus global land service; CRO, croplands; C_{ws}, water stress coefficient; DAAC, distributed active archive center; DBF, deciduous broadleaf forest; DIDSSF, daily integrated downward surface shortwave flux; DMET, daily MSG evapotranspiration; DMETREF, daily MSG reference evapotranspiration; DSSF, downward surface shortwave flux; ε, light use efficiency; ε_{max}, maximum light use efficiency; EBF, evergreen broadleaf forest; EC, eddy covariance; ECV, essential climate variables; ENF, evergreen needleaf; EO, earth observation; EPS, EUMETSAT polar system; ET, evapotranspiration; ET0, reference evapotranspiration; EUMETSAT, European organization for the exploitation of meteorological satellites; f_{APAR}, fraction of absorbed photosynthetically active radiation; GDMP, gross dry matter productivity; GLC2000, global land cover 2000; GPP, gross primary production; GRS, grasslands; LAI, leaf area index; LP, Land processes; LSA SAF, land surface analysis satellite application facility; MAD, mean absolute difference; MAE, mean absolute error; MBD, mean bias difference; MBE, mean bias error; MDFAPAR, MSG daily fraction of absorbed photosynthetic active radiation; MDGPP, MSG daily gross primary production; MGPP, MSG 10-day gross primary production; MODIS, moderate resolution imaging spectroradiometer; MSG, meteosat second generation; MXF, mixed forests; NASA, national aeronautics and space administration; RMAD, relative mean absolute difference; RMD, root mean difference; RMSD, root mean square difference; RMSE, root mean square error; R_{NIR}, near infrared reflectance; R_R, red reflectance; SAF, satellite application facility; SAV, savanna; SEVIRI, spinning enhanced visible and infrared imager; SMAP, soil moisture active passive; SHR, shrublands; PAR, photosynthetically active radiation; PET, potential evapotranspiration; PROBA-V, project for on-board autonomy

* Corresponding author.
E-mail address: beatriz.martinez@uv.es (B. Martínez).

https://doi.org/10.1016/j.isprsjprs.2019.11.010
Received 20 February 2019; Received in revised form 12 September 2019; Accepted 12 November 2019
Available online 29 November 2019

products is conducive to meet user needs for a better understanding of ecosystem processes and for improved understanding of anthropogenic impact on ecosystem services.

1. Introduction

A major awareness of the necessity of an improved monitoring of the global climate system is conducting for increased understanding of climate change and also for combating, monitoring and predicting severe events. This implies definition, establishment and quality assessment of Essential Climate Variables (ECV) products, which can be retrieved from Earth Observation (EO) at global scale (Bojinski et al., 2014). The Land Surface Analysis SAF (LSA SAF) is part of the Satellite Application Facility (SAF) network of European Organization for the Exploitation of Meteorological Satellites (EUMETSAT). It contributes to the monitoring of the biosphere from space since the end of 2008 with an ensemble of operational products, including ECVs such as the leaf area index (LAI), the fraction of absorbed photosynthetically active radiation by vegetation (f_{APAR}) and the fractional vegetation cover (https://landsaf.ipma.pt) (Trigo et al., 2011). The LSA-SAF products take benefit of EO data from sensors onboard EUMETSAT geostationary and polar orbiting satellites, such as the Spinning Enhanced Visible and InfraRed Imager (SEVIRI) on board of the Meteosat Second Generation (MSG) platform and the Advanced Very High Resolution Radiometer (AVHRR) aboard the EUMETSAT Polar System (EPS) (García-Haro et al., 2018), respectively.

Although not included in the ECVs list from the World Meteorological Organization, the gross primary production (GPP) is a relevant variable that measures the carbon uptake by photosynthesis per unit of time and area and thus it is directly connected with the amount of carbon dioxide in the atmosphere and some other atmospheric and terrestrial ECVs (GTOS, 2010; Bojinski et al., 2014).

In particular, for terrestrial biosphere, the continuous monitoring for improved understanding of the spatiotemporal variability in the GPP is essential for advancing our knowledge of global terrestrial carbon cycling and assessing the response to ongoing climate change (Zhang et al., 2014), especially for policy decision-making (Metz et al., 2006). Additionally, spatially explicit estimates of plant productivity are necessary for agricultural management and yield forecasting (Kang et al., 2009; Gitelson et al., 2014), assessing the contribution of forest ecosystems as main sinks of atmospheric carbon in the biosphere (Metz et al., 2006; Gilabert et al., 2017), or analyzing the response of ecosystems to extreme droughts (Vicca et al., 2016), among others.

Today technically feasible methods make EO-based GPP monitoring on a global scale applicable, and it thereby fulfill requirements for being an ECV (Bojinski et al., 2014). The first publicly available regular GPP product was the MOD17 (Heinsch et al., 2006; Zhao et al., 2011; Running and Zhao, 2015) from Moderate Resolution Imaging Spectroradiometer (MODIS). It corresponds to an 8-day global GPP composite at 1-km (version 5.5) and at 500-m (version 6) spatial resolution. A renewed interest for operationally derived GPP estimates at global scale entirely driven by EO data has emerged (Running et al., 2004), and a series of EO-based GPP products and initiatives at global scale are thereafter available, such as the monthly FLUXCOM product at 0.5° × 0.5° spatial resolution (Tramontana et al., 2016) from the Max Planck Institute for Biogeochemistry, the 10-day Gross Dry Matter Productivity (GDMP) product at 1 km (CGLOPS1, 2018a) from the Copernicus Global Land Service (CGLS) or the daily Soil Moisture Active Passive (SMAP) Level-4 carbon (L4_C) product at 9 km (Jones et al., 2017; Kimball et al., 2017) from National Aeronautics and Space Administration (NASA).

The absolutely most commonly applied method for predicting GPP using EO data at different spatial and temporal scales is the Monteith light use efficiency approach (Monteith, 1972; Waring and Running, 2007; Running and Zhao, 2015; Martínez et al., 2018a). According to this approach, the GPP is directly related to the absorbed photosynthetically active radiation (APAR), with ε as the proportional light use efficiency factor. APAR is given by the product of the f_{APAR} and the inward photosynthetically active radiation (PAR), whereas ε is modeled as the product of a ε_{max}, corresponding to the canopy functioning under best conditions, and a series of factors quantifying the reduction of photosynthesis as a consequence of different stresses such as water stress and thermal stress. Such a parameterization is currently adopted by the MOD17 (Heinsch et al., 2006), the GDMP (CGLOPS1, 2018b), and the SMAP L4_C products (Kimball et al., 2017). Frequently ε is also known as efficiency conversion since ε_{max} also takes into account the unit conversion from energy (APAR) to mass (GPP).

Given the importance of GPP for the monitoring of the terrestrial biosphere and its response to climate change, a consortium of EO-based GPP products is of high societal relevance. Today, the publicly available EO-based products are either based on MODIS (MOD17 and SMAP L4_C) or Project for On-Board Autonomy (PROBA-V) (GDMP) data. For the spatially explicit GPP to be properly assessed, it is extremely important that monitoring products are independent and based on different input data. The overarching aim of this study is to describe a completely new and recently launched 10-day GPP product based on data from the geostationary MSG satellite. In the current study, the physically based Monteith light use efficiency approach (Monteith, 1972) is applied, taking advantage of the suite of LSA-SAF products. The quality and robustness of the newly launched LSA-SAF GPP product (MGPP LSA-411) is evaluated at both site and global scales across the MSG disk using eddy covariance (EC) GPP estimates and EO-based GPP products, respectively.

The paper presents the following structure. The implementation of the modeling framework is described first. The MGPP product relies on: (i) an intermediate MSG daily GPP product (MDGPP) that aids to filter those unreliable observations when the 10-day GPP composite is computed and (ii) the use of a water balance to characterize the water stress factor in Monteith's approach. Secondly, the accuracy of the MGPP product is assessed against site-level GPP estimates from EC flux towers. Finally, a consistency analysis is performed by a direct comparison with other EO GPP products. These products are the 8-day MOD17A2H version-6 at 500-m spatial resolution, the daily 9-km SMAP (L4_C) product (SPL4CMDL) version 3 from NASA, and the 10-day GDMP product at 1 km from Copernicus.

2. MGPP retrieval methodology

2.1. Algorithm theoretical basis

The algorithm to retrieve 10-day GPP from SEVIRI/MSG data first computes daily GPP through Monteith's approach (Monteith, 1972). For this purpose, it uses two SAF products to obtain APAR: the DIDSSF, corresponding to the daily integrated downward surface shortwave flux (LSA-203), and the MDFAPAR, corresponding to the daily f_{APAR} LSA-SAF product (LSA-425). As previously mentioned, ε_{max} depends on the vegetation type. In this case, four main categories are considered corresponding to deciduous broadleaf forest (DBF), evergreen broadleaf forest (EBF), evergreen needleleaf forest (ENF), and mixed forest (MXF) and the remaining ecosystem types. On the basis of theoretical considerations (Garbulsky et al., 2010) and previous studies (Martínez et al., 2018a, 2018b), the assigned values to ε_{max} are: 1.8 g MJ^{-1}, 1.7 g MJ^{-1}, 1.5 g MJ^{-1} and 1.2 g MJ^{-1}, respectively. On the other hand, as radiation and water are the main climatic constraints to plant

growth at global scale (Nemani et al., 2003), only the water stress is considered. Thus, the Monteith approach to retrieve daily GPP (g m^{-2} day^{-1}) can be written as:

$$GPP = \varepsilon_{max} C_{ws} f_{APAR} PAR \quad (1)$$

where f_{APAR} is dimensionless and PAR is given in MJ m^{-2} day^{-1}. The water stress coefficient, C_{ws}, is obtained from a straightforward water balance from actual and potential evapotranspiration (AET and PET, respectively). The original C_{ws} was proposed by Potter et al. (2003) and applied satisfactorily over Italy (Maselli et al., 2009), Spain (Gilabert et al., 2015; Sánchez-Ruiz et al., 2017), and Euroafrica (Martínez et al., 2018a). A slight modification of C_{ws} is proposed in the MGPP algorithm:

$$C_{ws} = 0.6 + 0.4\frac{AET}{ET0} \quad (2)$$

where ET0 is the reference evapotranspiration. Two SEVIRI/MSG products are used in the calculation of C_{ws}, enhancing the internal consistency of the algorithm (see Section 2.2.3). The feasibility of taking into account the daily AET SEVIRI/MSG product (DMET, LSA 302) in the GPP algorithm was evaluated over Europe and Africa (Martínez et al., 2018a), providing a suitable solution to account for the water stress on vegetation at regional and global scales. It has been shown that the inclusion of the ET0 in Eq. (2) provides a reduction of the root mean square error (RMSE) up to 42% (Martínez et al., 2018a) as compared to MDGPP when the PET is considered (as proposed by Gilabert et al., 2015). As demonstrated by Martínez et al. (2018a), the C_{ws} parameterization achieves both the correct estimation of GPP in non-stressed areas and the downregulation of productivity during the dry season due to water scarcity.

C_{ws} ranges from 1 (no reduction, *e.g.* irrigated crops) to 0.6 (photosynthesis is reduced to 60% of its potential value due to short-term water scarcity). The use of daily AET and ET0 values in the algorithm is based on the following rationale: in order to avoid water loss when suffering water stress, plants close their stomata, which regulate both CO_2 and H_2O exchange with the atmosphere. Therefore, a quasi-immediate response to photosynthesis reduction due to a decrease in CO_2 diffusion can be expected in AET (Monson and Baldocchi, 2014).

The near-real time 10-day GPP values are derived from the mean of the daily GPP good quality values, which are obtained from the internal MDGPP product produced at daily temporal scale. The MGPP is produced at the LSA-SAF products grid; the native geostationary grid of SEVIRI with pixel size at the original resolution of SEVIRI/MSG (3 km at the sub-satellite point for standard channels). Further details are given in the Section 2.3.

2.2. Algorithm input data

2.2.1. PAR

The PAR, which designates the solar radiation from 0.4 μm to 0.7 μm, drives the process of photosynthesis. The MGPP algorithm computes the incoming daily PAR as 46% of the incoming global solar radiation (Iqbal, 1983) given by the MSG DIDSSF product (LSA-203), which is a daily integration of all the 30-min DSSF values. The DSSF represents the incident downward surface shortwave flux to the Earth's surface per area and time unit. It relies on surface albedo and atmospheric absorption, but most of all on cloud coverage and solar zenith angle (LSA SAF, 2012).

Several validation exercises of the DSSF product have been performed. Geiger et al. (2008) validated it in a ground measurement station placed in each of the following five European countries: Estonia, France, Portugal, Switzerland, and United Kingdom. Moreno et al. (2013) performed a more intense one using 45 ground stations of the Spanish meteorological agency (www.aemet.es) obtaining a mean absolute difference MAD = 11 W m^{-2} (6%).

2.2.2. f_{APAR}

The daily f_{APAR} product used in the algorithm (MDFAPAR) is provided by the LSA-SAF system over the SEVIRI/MSG projection (Camacho et al., 2017). It is linearly related to the Renormalized Difference Vegetation Index, obtained with the reflectance in the near infrared (R_{NIR}) and red (R_R) bands computed for an optimal geometry using the bidirectional reflectance distribution function (BRDF) parameters (Roujean et al., 1992; Roujean and Bréon, 1995). The error in the product generally ranges between 0 and 0.2. However, according to García-Haro and Camacho (2016), errors can be occasionally higher in Europe during wintertime due to a combination of effects (*e.g.* snow cover traces, large shadows, high cloud occurrence, high anisotropy, low illumination angles); whereas in Africa (with optimal acquisition geometry) only the persistent presence of clouds affects the uncertainty significantly (García-Haro and Camacho, 2016). According to Camacho et al. (2017), pixels with uncertainty greater than 0.15 should be labeled as poor quality ones.

The MDFAPAR product has showed to be consistent against ground measurements with an overall performance RMSE = 0.17 and 65% of samples within LSA-SAF target requirement level (Camacho et al., 2017). Overall discrepancies between MDFAPAR and equivalent products (*e.g.* SPOT/VGT GEOVI1 and MODIS15A2 C5) showed RMSE ≈ 0.16 and MBE ≈ –0.1 for the 2008–2009 period (Camacho et al., 2017).

2.2.3. Water stress coefficient (C_{ws})

The daily C_{ws} is calculated through the ratio between AET (DMET, LSA-302) and ET0 (DMETREF, LSA-303) LSA-SAF products. The ET0 is defined as the ET that a theoretical surface covered by green grass (0.12 m height) with a specific albedo, roughness length for heat and momentum, and surface resistance would have under particular atmospheric environment (Allen et al., 1998; Trigo and de Bruin, 2016). The DMETREF is derived using, as main input, the daily LSA-SAF shortwave radiation product at the surface (DIDSSF, LSA-203). The DMETREF product results from the combination of the thermodynamic model by Schmidt (1915) and a model for the atmospheric boundary layer (de Bruin et al., 2016).

According to Trigo and de Bruin (2016), the DMETREF product is appropriate for drought monitoring (among other large scale assessments) obtaining RMSE lower than 1.0 mm day^{-1} in temperate regions and up to 1.6 mm day^{-1} in dry and warm regions.

2.2.4. Maximum light use efficiency (ε_{max})

The 1-km Global Land Cover 2000 (GLC2000) (Bartholomé and Belward, 2005) is considered to assign the different biome-specific ε_{max} values. The GLC2000 legend development used the proposed Food and Agriculture Organization of the United Nations Land Cover Classification System (Di Gregorio and Jansen, 2000), which has been extensively considered in global land cover mapping. In fact, the GLC2000 land cover is a main input in the definition of boundaries among ecosystems such as forest, wetlands, and cultivated areas, which were defined by Millennium Ecosystem Assessment secretariat as priority land covers (http://www-gvm.jrc.it/glc2000/defaultGLC2000.htm) (Mayaux et al., 2006). The global map is obtained from regional products modified to the local conditions offering an overall accuracy of 68.6%, similar to other land cover maps, such as the International Geosphere Biosphere Programme (66.9%) or Globe Cover 2009 (67.5%) (Congalton et al., 2014).

A more general land cover was proposed by combining analogous classes from the original GLC2000. Therefore, the study area was characterized by 8 land cover classes: bare soil with an occurrence of 32% followed by croplands and grasslands with a presence of 15%. The forest land covers selected were deciduous broadleaf forest (13%), evergreen broadleaf forest (7%), evergreen needleleaf forest (2%), and mixed forest (5%). An 11% was obtained for the shrublands land cover. This simplification shortens the number of biomes though remaining the main geographical patterns (Martínez et al., 2013).

2.3. Algorithm implementation and outputs

Daily GPP (MDGPP) was calculated through Eqs. (1) and (2) using daily estimates of MDFAPAR, DIDSSF, DMET and DMETREF as input data. This daily product is currently operationally derived by the LSA-SAF system (*i.e.* internally disseminated) and corresponds to an improvement of that published in Martínez et al. (2018a). More detailed information regarding the performance of this daily product can be found in freely accessible documents (Martínez et al., 2018b, 2018c). The MGPP product was then computed from the mean value of high-quality daily MDGPP data (Fig. 1). Two quality requirements were used to assure the confidence of the 10-day product: (i) the occurrence of daily MDFAPAR errors smaller than 0.15 and (ii) the presence of gaps in the DIDSSF product lower than 5 days.

An error estimate of the 10-day GPP product was derived founded on the contribution of the relative errors of the input data. However, the existing MGPP product provides a theoretical error approximation by the addition of the different uncertainties associated only to the f_{APAR} product (MDFAPAR). If the errors published by Moreno et al. (2013) (*e.g.* rMBD ≈ 1%) are considered, the PAR relative error could be disregarded as compared to the relative uncertainty of the MDFAPAR product (with a relative uncertainty of 10%). Furthermore, the light use efficiency error is determined by the ε_{max} and C_{ws}, which show the same order of magnitude that the f_{APAR} error (Gilabert et al., 2015).

The MGPP product consists of 4 different layers (Fig. 1). Layer 1 (MGPP) comprises the 10-day mean GPP value. Layer 2 (MGPP QF1) corresponds to the total of days with MDFAPAR uncertainty above 0.15 along the 10-day period. Layer 3 (MGPP error) informs us about the associated MGPP error whereas layer 4 (MGPP QF2) refers to the total of daily MDGPP images considered in the MGPP estimation. A high confidence of the MGPP product would be expected for low MGPP QF1 and high MGPP QF2 values, respectively. The MGPP product is only delivered when more than three MDGPP images are available (see example in Fig. 1).

3. MGPP assessment

The MGPP product assessment was achieved based on the main recommendations suggested by the Land Product Validation of the Committee on Earth Observation Satellite Working Group Cal/Val for validation of the EO-based products (Fernandes et al., 2014). This comprises different exercises for the assessment of moderate and coarse resolution EO-based products:

(i) The MGPP global patterns consistency was analyzed. General global patterns and seasonal dynamics were qualitatively evaluated for the MGPP along with the different EO-based GPP products. This qualitative assessment provided us information about the capability of the MGPP product to reproduce global patterns and seasonality in order to determine any apparent MGPP model errors or anomalies.

(ii) The MGPP performance was assessed against site-level EC flux estimates, which provide estimates of the product accuracy. This validation relied on the correlation coefficient (r), the mean absolute error (MAE), the mean bias error (MBE), and the root mean square error (RMSE). The latter three quantities expressed in g m^{-2} day^{-1}. The Appendix A shows a summary of the performance of the daily product (MDGPP) used to derive the MGPP, which was assessed against daily EC estimates.

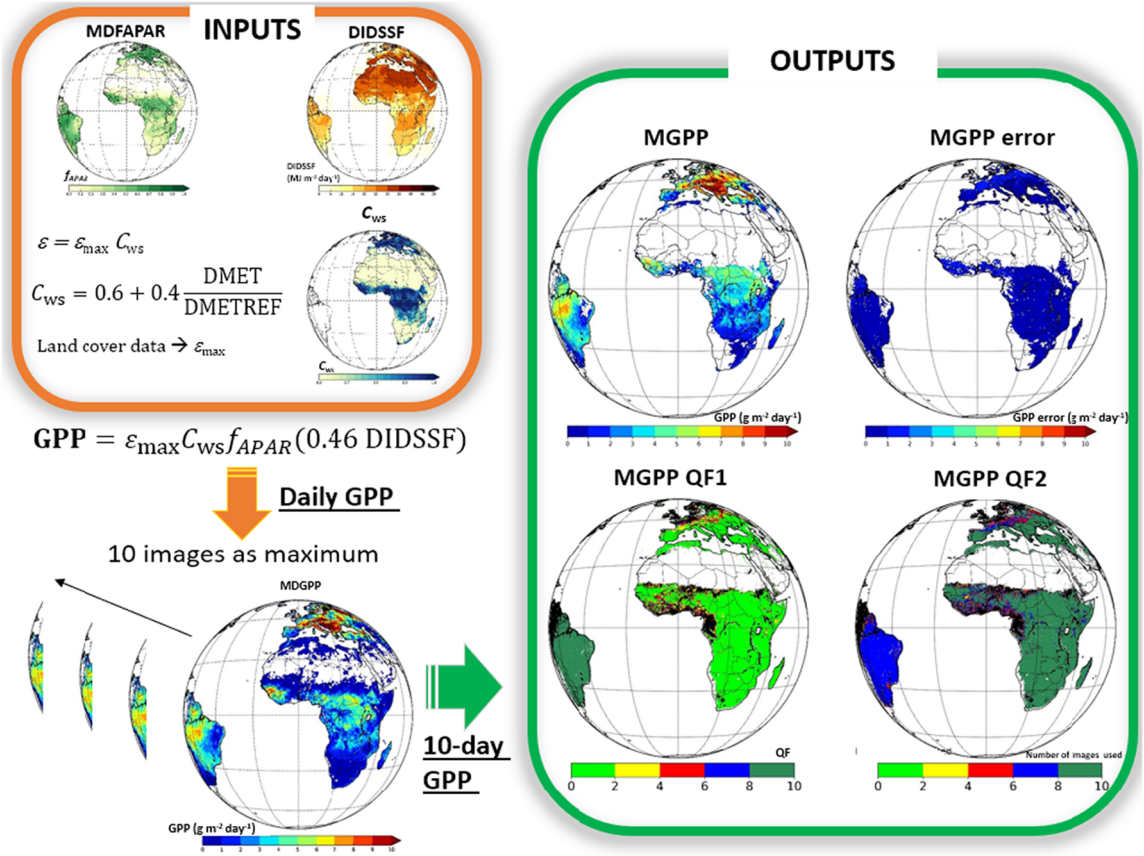

Fig. 1. Scheme of the methodology proposed to derive the MGPP product for a particular date. The required inputs of the algorithm are depicted inside the orange frame whilst the different MGPP layers are drawn inside the green. (For interpretation of the references to colour in this figure legend, the reader is referred to the web version of this article.)

(iii) The MGPP performance against global benchmarking EO-based GPP products was also accomplished to assess the MGPP product skills regarding the temporal and spatial reliability over the main land covers. The root mean square difference between products (RMSD), the mean bias difference (MBD), the mean absolute difference (MAD), and the correlation coefficient were considered to quantitatively assess the discrepancies between products. Lastly, the differences of the mean GPP values between the EO-based GPP products against latitude are analyzed by means of the Hovmoller diagrams. The differences are computed every 10°-latitude bands in each month during the period 2015–2017.

Finally, a user requirements compliance analysis at selected FLUXNET sites was achieved. Three categories were proposed based on the needs of user requirements defined in the LSA-SAF project and following different recommendations adopted from relevant studies (Schaefer et al., 2012; Kimball et al., 2016; Baldocchi, 2008). Consequently, three requirement levels were proposed based on different ranges computed from the GPP residuals of the EO-based products and the EC flux towers GPP estimates: optimal accuracy for residuals values below 1.0 g m^{-2} day^{-1}, target accuracy for residuals below 2.0 g m^{-2} day^{-1}, and threshold accuracy for residuals values below 3.0 g m^{-2} day^{-1}.

4. Data for MGPP assessment

4.1. EC tower GPP estimates

A spatial analysis to quantify MSG pixel homogeneity was conducted over all FLUXNET EC towers within the MSG disk. The land cover similarity within a 5 × 5 km^2 area around the towers was investigated using the 1-km GLC2000. Those sites that showed more than two land cover types were neglected for the MGPP assessment. The fraction of every land cover inside the considered 5 × 5 km^2 area was computed. Sites with a land cover fraction above 80% were considered directly. The rest of the sites were analyzed using Google Earth by visual inspection. In the end, 8 sites were selected for the study (Table 1 and Fig. 2 left). The pixel purity of the 5 × 5 km^2 area was computed as the fraction of the most dominant land cover. Daily GPP data from these sites were provided by the principal EC tower responsibles. The process to derive GPP estimates for every site comprised the gap filling of net ecosystem exchange time series along with the application of a standard flux partitioning algorithm (Lasslop et al., 2010). The GPP estimates were averaged for each 10-day period and compared with the MGPP estimates.

Fig. 2 (right) displays the location of different sites (MSGVAL) used to achieve the comparison between MGPP and the other EO-based GPP products (Fuster et al., 2017). The MSGVAL consists of 478 sites that characterize the global variability of different land surface types: 239 BELMANIP-2.1 (Weiss et al., 2014) sites covering the MSG disk, 120 EUVAL sites located over Europe and North of Africa (Camacho et al., 2017), 29 African validation sites used by the Natural Resources Monitoring for Africa throughout geoland-2 project, 8 Enviro-Net sites (www.enviro-net.org/) over South of America, 63 sites proposed in OLIVE DIRECT (http://calvalportal.ceos.org), and 19 used in the FP7 ImagineS project (http://fp7- imagines.eu/).

4.2. EO-based GPP products

4.2.1. MODIS GPP product (MOD17A2H)

The 8-day MODIS GPP product version 6 (MOD17A2H V006) at 500-m spatial resolution was obtained from the online NASA archive, the Land Processes (LP) Distributed Active Archive Center (DAAC), (https://reverb.echo.nasa.gov). The V006 products use the same algorithm as MODIS GPP version-5 (Zhao et al., 2005, Zhan and Running, 2010) but with some improvements concerning the use of: (i) a higher spatial resolution (500 m) since the 8-day composite LAI/FPAR MODIS product at 500-m resolution is used, (ii) an updated Biome Property Look Up Table (BPLUT) and (iii) an updated version of the meteorological data from the Global Modeling and Assimilation Office.

The MODIS product was reprojected to the SEVIRI/MSG disk by considering all the MODIS values within a SEVIRI pixel and labeled as acceptable quality control. This version includes some cloud-contaminated LAI/FPAR inputs that users are recommended to reject by considering the quality information contained in the product. In our case, the quality control provided by the product (layer 3) was used to discard those pixels with poor and unacceptable quality. Those pixels corresponded mainly to snow, water or unreliable values.

4.2.2. SMAP GPP product (SPL4CMDL)

The SMAP Level-4 carbon (L4_C) product (SPL4CMDL) version 3 provides 9-km global gridded daily estimates of GPP derived by using SMAP L-band microwave data and different information (e.g. land cover and vegetation) derived from MODIS, Visible Infrared Imaging Radiometer Suite, and the Goddard Earth Observing System Model land model integration scheme.

The L4_C algorithm is mainly based on the MOD17 algorithm (Zhao et al., 2005, Zhao and Running, 2010) but modified to inputs in a daily basis (Kimball et al., 2009, Yi et al., 2013). The L4_C calculations are first conducted at a 1-km spatial resolution agreeing with other inputs such as f_{APAR}. Only best quality f_{APAR} data are included as L4_C inputs. Absent or poor quality 8-day f_{APAR} data are refilled by using the values of a typical climatological f_{APAR} dataset derived from a 10 years long-term MODIS f_{APAR} data record. Thus, this auxiliary MODIS f_{APAR} at 8-day allows a backup option to fill the missing values in the SMAP product.

The SPL4CMDL product performance was successfully tested against reference flux measurements (e.g. FLUXNET EC) and synergistic global remote sensing products (e.g. GPP from Max Planck Institute) covering different latitudinal, land cover and vegetation biomass conditions (Kimball et al., 2014).

The SMAP data were re-projected from the cylindrical 9-km Equal-

Table 1
Detailed information of the 8 EC sites selected over Europe and Africa. The pixel purity over a 5 × 5 km^2 GLC2000 area is also included. In accord with the FLUXNET site information, the different land covers considered correspond to: DBF (deciduous broadleaf forest), EBF (evergreen broadleaf forest), ENF (evergreen needleleaf forest), MXF (mixed forest), SHR (shrublands), CRO (croplands), GRS (grasslands) and SAV (savanna).

Site	Name	Country	Latitude (°)	Longitude (°)	Altitude (m)	Land Cover	GLC2000	pixel purity	Temporal coverage	Reference
DE-Geb	Gebessee	Germany	51.10	10.91	161	CRO	CRO	100	(01/2015–12/2017)	Anthoni et al. (2014)
DE-Gri	Grillenburg	Germany	50.95	13.51	385	GRS	ENF	92	(01/2015–12/2017)	Hussain et al. (2011)
DE-Kli	Klingenberg	Germany	50.89	13.52	478	CRO	CRO	100	(01/2015–12/2017)	Preschet et al. (2010)
DE-Tha	Tharandt	Germany	50.96	13.57	385	ENF	ENF	60	(01/2015–12/2017)	Preschet et al. (2010)
ES-LMa	Las Majadas	Spain	39.94	−5.77	258	SAV	MXF	80	(01/2015–09/2017)	Casals et al. (2011)
FI-Hyy	Hyytiala	Finland	61.85	24.29	181	ENF	ENF	80	(01/2015–12/2017)	Suni et al. (2003)
SN-Dhr	Dahra	Senegal	15.40	−15.43	40	SAV	CRO	100	(01/2015–12/2017)	Tagesson et al. (2015a)
Za-Kru	Skukuza	Southafrica	–25.02	31.50	359	SAV	SHR + DBF	64	(12/2015–12/2017)	Archibald et al. (2009)

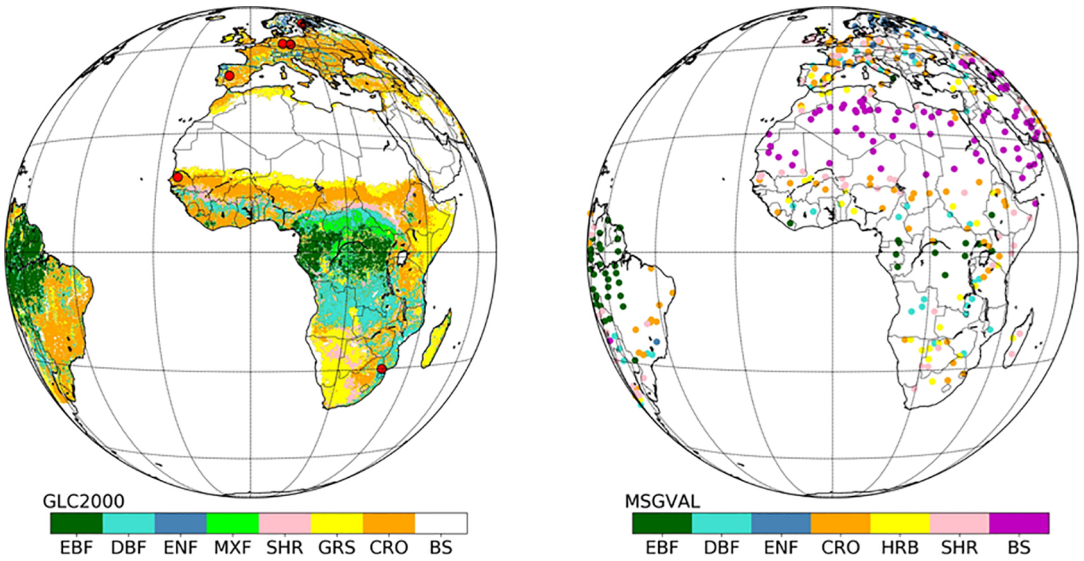

Fig. 2. Left: The Global Land Cover 2000 (GLC2000) adapted to the SEVIRI projection. The considered EC towers are also depicted in red points. A more general classification of 8 land classes has been obtained to decrease the 23-land cover types though conserving the main characteristics of the original GLC2000. **Right**: MSGVAL network location at different land covers for comparison between MGPP and other EO-based GPP products (Fuster et al., 2017).

Area Scalable Earth Grid, version 2.0 (EASE-Grid 2.0) to the geographic 1-km (WSG-84) projection. The resulting SMAP data in geographic coordinates were geo-located to the normal SEVIRI projection by a similar process applied to the MOD17A2H product.

4.2.3. Copernicus GDMP

The 1-km GDMP product provides global 10-day estimates of GPP based on SPOT-VEGETATION and PROBA-V data. The Monteith approach is used to derive the GDMP product of the CGLS. It is an intermediate product for the dry matter product (DMP) V2 that is delivered to users. It is related to the total of biomass that is produced in a specified length of time, without considering any diminution caused by other processes, such as plant respiration. This product uses the CGLS f_{APAR} version 2 as an input, which shows a smaller amount of missing values conferring the GDMP product a smoother time series with higher continuance with respect to version 1 (CGLOPS1, 2018b). One of the main features of the GDMP V2 concerns the use of specific ε_{max} values per biome obtained by adjusting the GDMP values with EC GPP estimates (*i.e.* 224 FLUXNET towers globally distributed). However, water stress factors are not directly accounted for in the DMP prototype, considering that it is inherently accounted for the f_{APAR}. The GDMP data at 1 km were geo-located to the native SEVIRI system by a similar process as for the MODIS data.

5. Results

5.1. MGPP global patterns and features

Fig. 3 shows the mean values for the MGPP, MODIS, SMAP and GDMP at SEVIRI/MSG spatial resolution for January, April, July and October 2015–2017. The GPP products were computed at monthly temporal resolution by averaging the good quality GPP values in a monthly step. The monthly average for every product was computed when more than three images were available. Areas in white belong to pixels where the MGPP product did not provide valid values (e.g. water and snow pixels and pixels with no valid inputs values). GPP values were not provided at desert areas owing to the absence of required products in Eq. (1) (e.g. AET).

In general, all the GPP products showed spatially consistent patterns. As expected, higher GPP values were produced over forests (e.g. rainforest regions and pixels located at latitudes around 50°–60°N), whereas low GPP values were observed over drylands regions (e.g. southern Spain, Sahel region, eastern Africa and southern Africa). Discrepancies between the GDMP and the rest of the products were clear and the GDMP values were much higher than the other products. Although differences existed among all products, MGPP, MODIS and SMAP GPP estimates provided lower relative differences as compared to GDMP. The MGPP product provided higher values over tropical forests in central Africa than the MODIS and SMAP products. Indeed, a recently study has reported inaccuracies in the MOD17 GPP collections 5.0, 5.5 and 6.0 over tropical forests (De Almeida et al., 2018). A larger number of gaps were observed in the MGPP product due to the no availability of f_{APAR} values throughout wintertime at very high latitudes ($> 50^{\circ}$ N) and West regions of central Africa, whereas the SMAP and GDMP products provided fewer missing values since the retrieval algorithms used different gap filling methods.

The seasonal variation in the quality of the MGPP product during the period 2015–2017 is depicted in Fig. 4. The quality (good, medium, poor and bad) was computed based on the coverage of the product during the considered period. Overall, a high mean coverage (around 80% of pixels) of good and medium quality observations was presented for all the period (green and turquoise colors in Fig. 4 left). Only around the 6% of MSG disk showed poor consistency (red colors) for all the period. More excluded values were observed at the beginning and end of the year (around 15%) mainly due to the combination of reduced incoming PAR, increased anisotropy, persistent presence of clouds and snow cover at high latitudes in the North hemisphere (García-Haro et al., 2018). The best performance corresponded to areas located under 40°N latitude, as African continent and southern Europe, whereas poor and bad quality levels were observed at the edge of the disk such as in northern Europe and central South America.

5.2. MGPP performance against EC tower GPP estimates

The MGPP profiles captured the seasonal dynamics in GPP throughout the year, particularly in the off-growing season, indicating that the algorithm was responding to short-term changes in environmental conditions (Fig. 5). However, the magnitude of the MGPP was not always precise; at croplands and grassland flux tower sites (DE-Geb, DE-Kli and DE-Gri), a RMSE > 3 g m^{-2} day^{-1} was observed. These sites were strongly influenced by management practices. For example, the grassland is harvested two to four times per year, which explains the

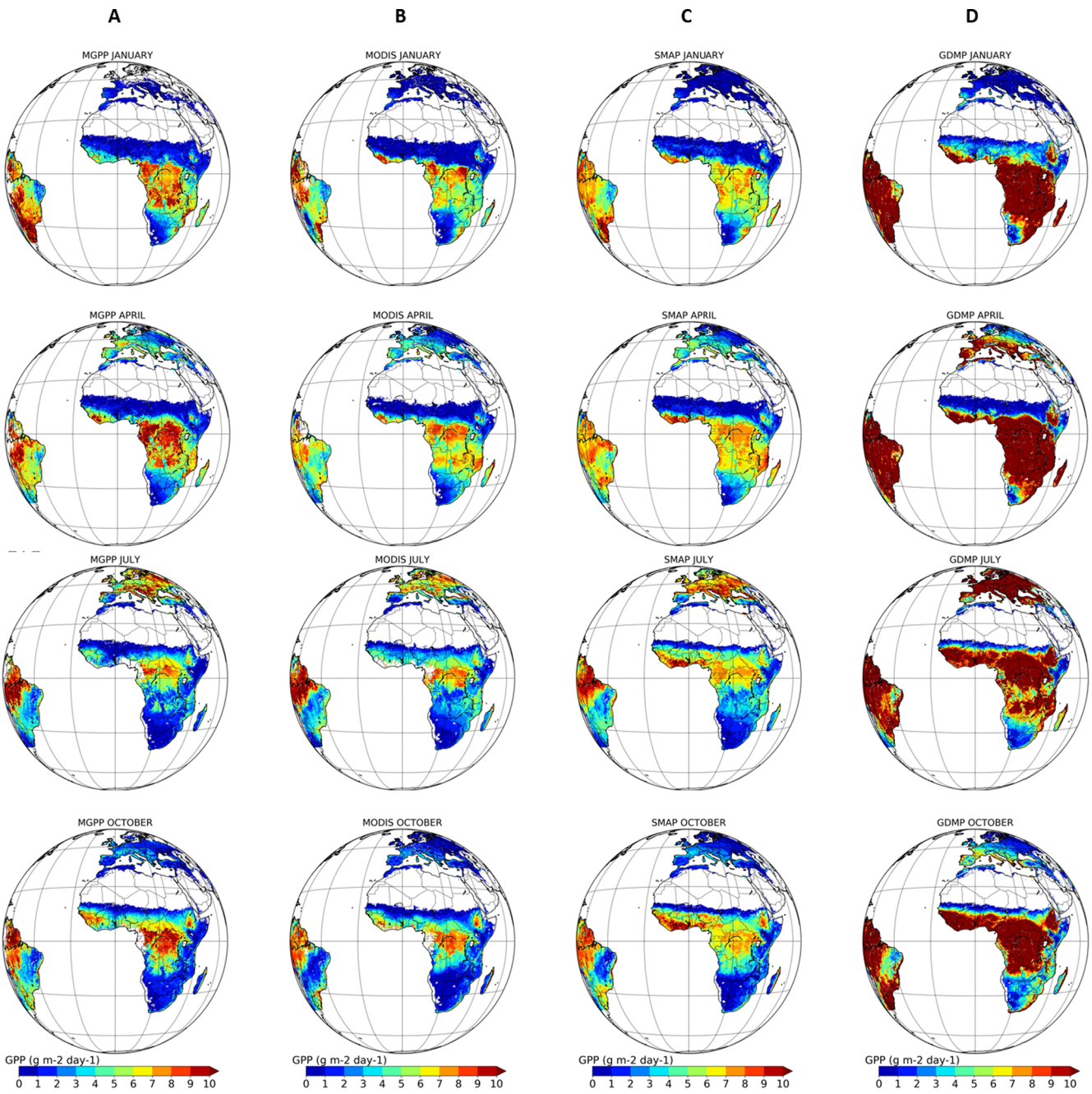

Fig. 3. GPP mean values from 2015 to 2017 for January, April, July and October (rows) at MSG disk for MGPP, MODIS, SMAP, and GDMP products (columns A, B, C, and D, respectively).

sudden drops in the EC GPP observed during the central part of the maximum vegetation development for 2016 and 2017. Neither of the EO-based products was able to reproduce these sudden drops at DE-Gri grassland site whereas MGPP, MODIS and SMAP reproduced the harvest at the crop sites well. The start of the growing season was well reproduced by all EO products. Although the GDMP product better agreed with the EC GPP during the growing season onset, it was not able to reproduce neither the relatively rapid diminution during the middle of the year nor capture the inter-annual changes on GPP observed in DE-Kli site at the end of the period. For the crop sites (DE-Gri and DE-Kli), the MGPP product achieved the best validation metrics of the EO GPP products (Table 2).

At the evergreen needleleaf forest sites (DE-Tha and FI-Hyy), the MGPP performed well and again had the best validation metrics of the EO-based GPP products (Table 2). Both sites belong to a very homogeneous area, mainly composed by coniferous evergreen species (Suni et al., 2003; Preschet et al., 2010). The GDMP product had again a very different magnitude as compared to the other products, which may be partially explained by the $\varepsilon_{max.}$ A higher ε_{max} value (1.98 g m^{-2} day^{-1}) is assigned in the GDMP algorithm as compared to the rest of the products (1.5 g m^{-2} day^{-1} for MGPP and 0.96 g m^{-2} day^{-1} for MODIS and SMAP).

The savanna site (ZA-Kru) inside the Kruger National Park is a good example for the potential of MGPP to detect drought events. Savanna ecosystems cover about fifth of the Earth's land surface and just under half of Africa's land area. Thus, monitoring changes in savannas requires a method that may offer sufficiently large spatial extents (Tsalyuk et al., 2017). At this site, an extremely strong El Niño caused a major drought (precipitation of 185 mm, below its average of 550 mm) in the growing season of 2015/2016, which was comparable with the

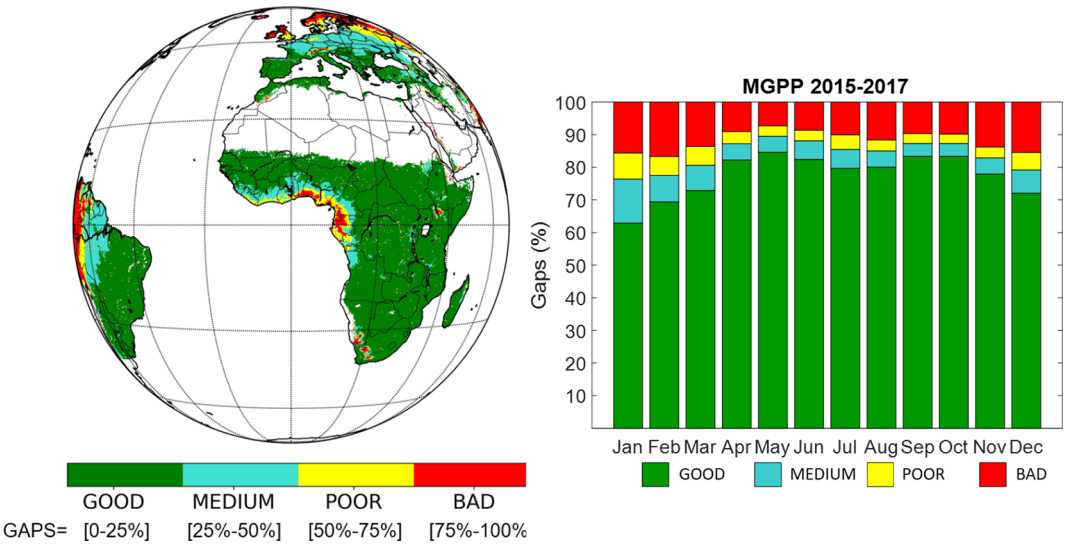

Fig. 4. Quality of the MGPP product as a function of the mean gaps for the 2015–2017 period (left). Quality of the MGPP product per month for the 2015–2017 period (right).

1933 and 1982 droughts in southern Africa (Bahtaa et al., 2016). All EO products showed low GPP during this drought event (Fig. 5). A higher increase in EC GPP was observed during the growing season of 2017 that was only reproduced by the GDMP product. MGPP, MODIS and SMAP products showed similar GPP values for all the considered period. The MGPP product also reproduced the low GPP values as caused by low precipitation levels at the site in Spain (ES-LMa). The year 2017 was identified as the second driest year since 1965 (2005 was the driest) with a mean annual precipitation of 474 mm, which is 27% lower than the mean annual value (1981–2010) (http://www.aemet.es/es/serviciosclimaticos/). The MGPP product reproduced the EC GPP measurements most accurate followed by the MODIS and SMAP products (Table 2). The GDMP product again produced too high peak values with GPP outcomes up to 20 g m^{-2} day^{-1}.

The savanna site at Dahra (SN-Dhr) showed typical seasonal dynamics of semi-arid sites with low GPP throughout the dry season and peak values along the wet period (Fig. 5; Tagesson et al., 2015). However, the ground-based measurements of GPP reached values around 14 g m^{-2} day^{-1}, which was much higher than GPP usually found in semi-arid savanna ecosystems (Tagesson et al., 2016) explaining why all EO-based products showed a lower magnitude than the field measured values. The GDMP and MGPP products reproduced the site GPP better than SMAP and MODIS (Fig. 6; Table 2). It can be appreciated in Fig. 6 that GDMP generally overestimates EC observations, while the rest of the products underestimate them. Exceptions are MGPP, MODIS, and SMAP overestimating low GPP in DE-Geb and DE-Kli.

5.3. MGPP performance against global benchmarking EO-based GPP products

Scatterplots between the MGPP and MODIS (left), SMAP (center) and GDMP (right) products for the MSGVAL network are shown in Fig. 7 for the period 2015–2017. Colors refer in this case to the different continents, Europe (blue), Asia (black), Africa (red) and South America (green). Overall, the largest discrepancies were observed for the three land covers of forest with the lowest error between MGPP and SMAP (RMSD $<$ 2.1 g m^{-2} day^{-1}) and the highest error between MGPP and GDMP (RMSD $<$ 12.2 g m^{-2} day^{-1}) (Table 3). In the last case, the GDMP had significantly different GPP distribution values as compared to the MGPP. The MGPP values provided lower values than the GDMP product (majority of the points are distributed under the centerline, dashed black line), which was in accordance with findings in Fig. 3. The lowest differences were observed for the other land covers (i.e. herbaceous (HRB), shrublands (SHR), croplands (CROP), and bare soil (BS)) with a major concordance between MGPP-MODIS and MGPP-SMAP (i.e. lower differences between estimates and similar regression parameters values). The BS results have to be considered with caution since the number of observations was lower than for the analysis with the other land covers. A slightly better agreement was observed between MGPP and SMAP as compared to MODIS, maybe partly explained by the original coarser SMAP spatial resolution (9 km). The distribution of locations according to the different continents was as expected. Higher GPP values of all the products for EBF over Africa (red) and South America (green), main contribution of Europe and South America for ENF and equal influence of all of continents to HRB, SHR and CROP land covers.

Fig. 8 shows the Hovmoller diagrams of differences of the mean GPP values between the EO-based GPP products against latitude in each month during the 2015–2017 period. The MGPP product showed a good agreement with MODIS products over most of the latitudes with the lowest MBD (MBD $<$ 2 g m^{-2} day^{-1}). Larger differences were observed between MGPP and SMAP (MBD $>$ 6 g m^{-2} day^{-1}), particularly at latitudes $>$ 40° N and over rainforest regions below the equator. These differences tended to zero during winter season (red colors), first months in the northern hemisphere and middle of the year for the southern hemisphere, whereas they increased during summer season (green and yellow colors). The MBD between MGPP and GDMP showed negative values in the majority of the analyzed latitude values, indicating larger GDMP values for all the considered period as observed in previous sections.

5.4. User requirements compliance

The number of observations (percent value) with a residual between MGPP and EC GPP estimates falling below the optimal ($<$ 1.0 g m^{-2} day^{-1}), target ($<$ 2.0 g m^{-2} day^{-1}) and threshold ($<$ 3.0 g m^{-2} day^{-1}) values were computed. The percentage for MODIS, SMAP and GDMP was also computed for reference. For MGPP, the 48% of cases was found below the optimal accuracy as opposed to the 36%, 43% and 40% found for MODIS, GDMP and SMAP products, whereas a 64% of the measurements were below the target accuracy. Although only 75% of the observations were within the threshold user requirement, this value agreed with those observed for MODIS, GDMP and SMAP products (75%, 76% and 74%, respectively). This accuracy was increased to 81% when croplands (DE-Geb and DE-Kli) were not

considered. Schaefer et al. (2012) stated that models' performance was superior at forest and worse at croplands, grassland and savanna sites. This may be explained by the fact that at croplands landscapes, the worst accord was found between the flux tower footprint (usually < 1 km) and the EO-based products footprint mainly due to patchy landscapes at large-scale (Baldocchi, 2008).

6. Discussion

Several factors that could explain MGPP disagreements with site-level EC GPP estimates or EO-based GPP products are identified from the results as: cloud-contaminated f_{APAR} estimates, ε parameterization, ε_{max} assignments to the different biome, a wrong assignment of GLC2000 or a spatial resolution mismatch between the EO-based GPP products and the site-level EC GPP footprint. In this concern, the discussion of the MGPP performance is emphasized in terms of four major key issues of the algorithm:

(i) Light use efficiency parameterization

The ε considered in the Monteith approach underlies environmental constraint metrics representing the reduction of maximum carbon rate levels from potential conditions to unfavorable environmental and physiological constrains (Connolly et al., 2009; Gilabert et al., 2015). These environmental constrains refer to extreme daily air temperatures and low soil moisture among others (Kimball et al., 2016). The EO-based products considered in the assessment mainly include a series of factors quantifying the decrease of light use efficiency owing to water scarcity and very low temperature conditions.

The use of MGPP can take advantage from the consideration in the methodology of the reduction in efficiency due to water shortage such as the MODIS and SMAP products. Different studies (Yuan et al., 2007;

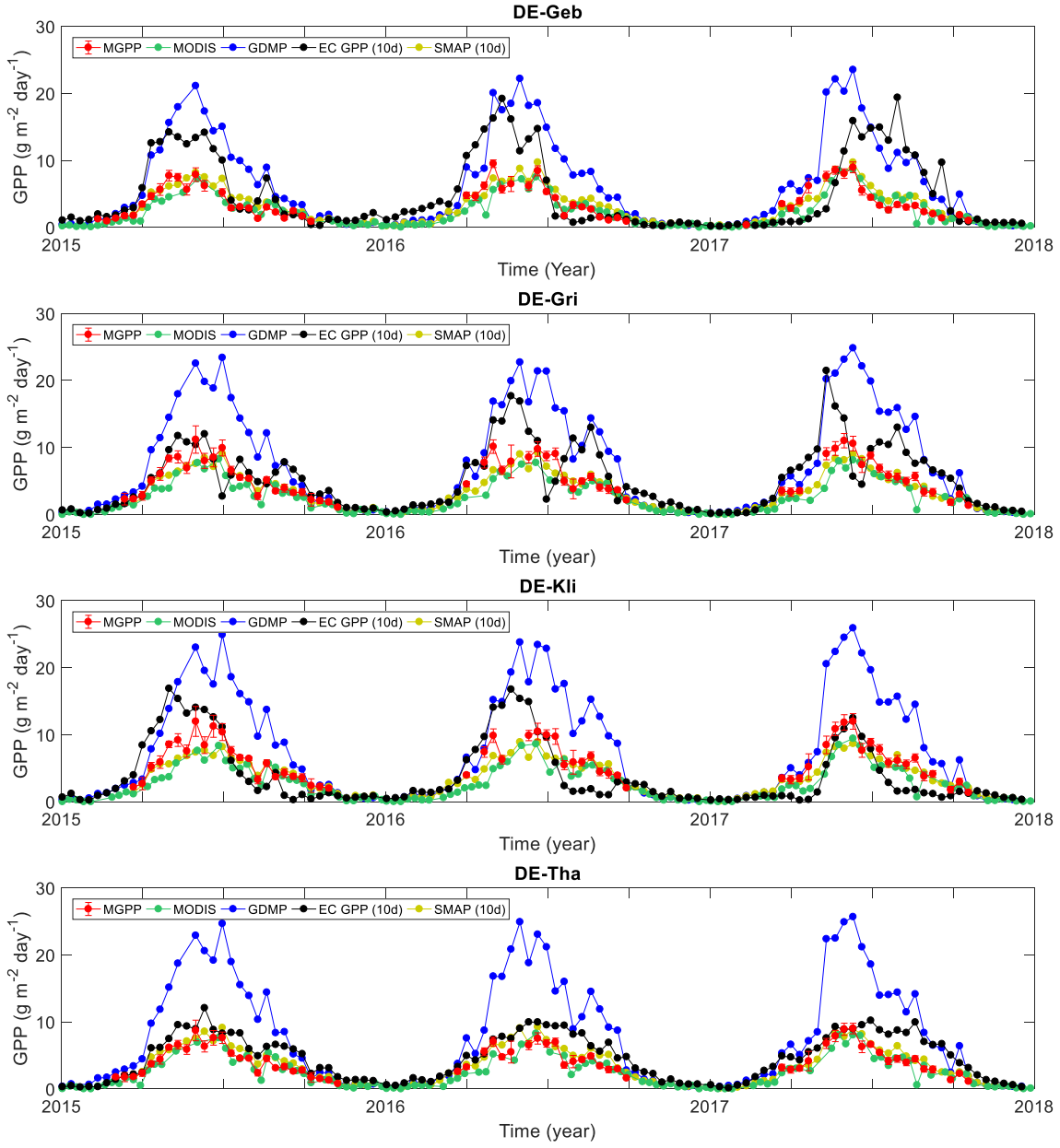

Fig. 5. Temporal profiles of 10-day MGPP (red dots) product together with EC tower GPP estimates (black dots) data at de different FLUXNET EC towers for 2015–2017. The MODIS (green dots), SMAP (yellow dots), and GDMP (blue dots) products were temporally resampled at 10-day resolution and also included for reference. All GPP products were spatially resampled using the MGPP product as reference. (For interpretation of the references to colour in this figure legend, the reader is referred to the web version of this article.)

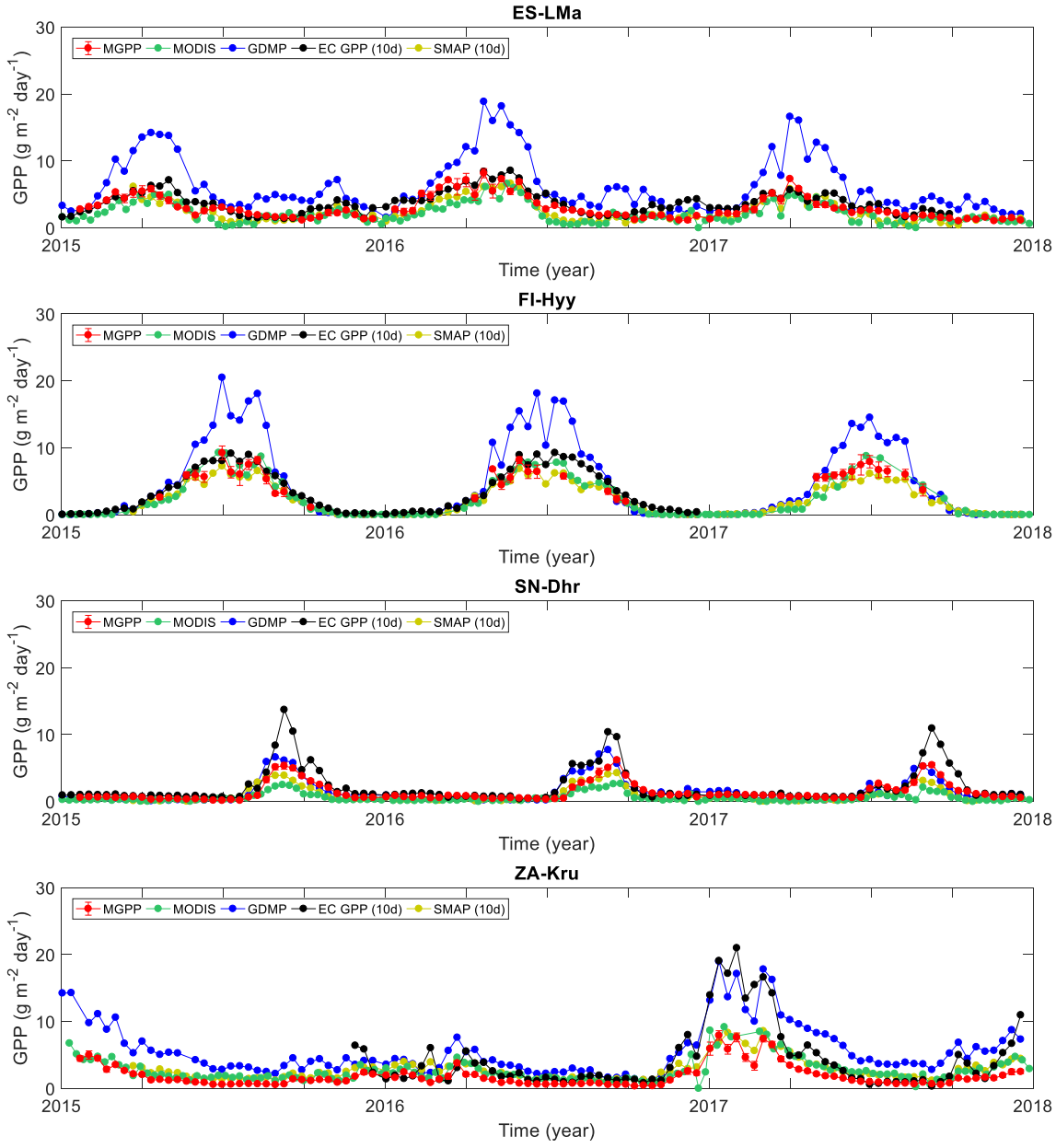

Fig. 5. (*continued*)

Garbulsky et al., 2010) stated that when vegetation is adapted to its local environment, water availability constrains more its function than temperature. Particularly, the MGPP product provides certain skill to deal with water stress throughout dry periods at sites in Africa (SN-Dhr and ZA-Kru). For ZA-Kru site, the MGPP, MODIS and SMAP profiles achieve a good agreement with the EC GPP data along the growing period when a reduction in water availability is supposed. However, higher GDMP values are observed for the dry season that could be explained by the fact that the GDMP algorithm does not include a water stress factor to account for short term drought stresses. These results agree with those observed in Fig. 6 for grasslands and shrublands. A similar overall low difference between MGPP and MODIS and between MGPP and SMAP is observed as opposed to the high dissimilarity between MGPP and GDMP (Table 2). These findings may be indicative of the water stress as a key factor to explain the differences and not the ε_{max} different assignment values (1.2 g MJ^{-1}, 0.9 g MJ^{-1} and 2.4 g MJ^{-1} for grasslands and 1.2 g MJ^{-1}, 1.3 g MJ^{-1} and 2.1 g MJ^{-1} for shrublands for MGPP, MODIS and GDMP, respectively). These results highlight the major role of the water balance through the AET/ET0 ratio as a constraining factor in the MGPP approach for semi-arid regions.

A potentially important factor such as thermal stress is omitted in the present version of the MGPP product. As a consequence, the MGPP product does not include the reduction in the GPP due to cold temperatures that could mainly affect regions at high altitudes and high latitudes. It might be argued that the thermal effects are manifested along winter season where very low GPP values are expected.

(ii) ε_{max} assignment

The MGPP model is based on the assumption that ε_{max} depends on the biome and is characterized using a global land cover classification. However, ε_{max} can show certain variability within specific biomes between different EO-based GPP products (Turner et al., 2002; Madani et al., 2014; Gitelson and Gamon, 2015) that can be a source of uncertainty in GPP estimation (Madani et al., 2014). This is the case of the GDMP product, which assigns a higher ε_{max} value for croplands (2.7 g MJ^{-1}) as opposed to MGPP (1.4 g MJ^{-1}), while other vegetation

Table 2
Results derived from the comparison between MGPP and EC tower GPP estimates. RMSE, MBE and MAE are written in g m^{-2} day^{-1}. The correlation between the EO-based GPP products and the EC GPP estimates is also computed.

Site	EO-based GPP product	MBE	MAE	RMSE	r
DE-Geb	MGPP	−3.4	4.3	5.7	0.67
	MODIS	−3.7	4.5	6.0	0.67
	SMAP	−3.2	4.5	5.8	0.64
	GDMP	2.4	4.3	5.5	0.66
DE-Gri	MGPP	−2.1	3.0	4.0	0.62
	MODIS	−3.5	4.0	5.0	0.55
	SMAP	−2.8	3.6	4.6	0.51
	GDMP	4.2	4.7	7.0	0.60
DE-Kli	MGPP	0.4	3.0	3.6	0.74
	MODIS	−1.3	3.4	4.5	0.57
	SMAP	−0.5	3.6	4.3	0.59
	GDMP	6.6	7.7	9.0	0.52
DE-Tha	MGPP	−2.2	2.3	2.7	0.80
	MODIS	−2.7	2.7	3.1	0.82
	SMAP	−1.8	1.8	2.2	0.86
	GDMP	5.1	5.4	7.2	0.85
ES-LMa	MGPP	−0.6	0.9	1.1	0.84
	MODIS	−1.5	1.5	1.7	0.88
	SMAP	−1.4	1.5	1.9	0.69
	GDMP	2.9	3.1	4.1	0.84
FI-Hyy	MGPP	−1.0	1.3	1.5	0.85
	MODIS	−0.7	0.9	1.1	0.93
	SMAP	−1.8	1.8	2.0	0.89
	GDMP	4.2	4.6	5.8	0.91
SN-Dhr	MGPP	−0.8	0.9	1.7	0.93
	MODIS	−1.6	1.6	2.7	0.89
	SMAP	−1.3	1.4	2.4	0.86
	GDMP	−0.7	0.9	1.6	0.87
ZA-Kru	MGPP	−2.3	2.4	3.9	0.91
	MODIS	−1.3	1.9	3.3	0.90
	SMAP	−0.8	1.3	2.0	0.77
	GDMP	1.3	2.1	2.5	0.89

Note: Correlations demonstrated a significance level up to 95%.

types are parameterized using similar ε_{max} values. For example, 1.4 g MJ^{-1} and 1.2 g MJ^{-1} for grasslands, and 1.9 g MJ^{-1} and 1.8 g MJ^{-1} for DBF by GDMP and MGPP, respectively.

The larger discrepancies are observed for the EC GPP estimates belonging to ENF (e.g. DE-Tha, DE-Gri and FI-Hyy) since both GDMP and MGPP algorithm differ in the ε_{max} assignment (1.9 g MJ^{-1} for GDMP and 1.5 g MJ^{-1} for MGPP). In this case, differences up to 150% are observed between the GDMP and the GPP from EC data for the growing season with large errors (RMSE = 7.2 g m^{-2} day^{-1}, RMSE = 7.0 g m^{-2} day^{-1} and RMSE = 5.8 g m^{-2} day^{-1}, respectively) as opposed to the lower differences (up to 50%) obtained between MGPP and GPP EC (RMSE = 2.7 g m^{-2} day^{-1}, RMSE = 4.0 g m^{-2} day^{-1}, RMSE = 1.5 g m^{-2} day^{-1}). This is in agreement with the findings of Table 3 for ENF land cover with mean differences up to 8.8 g m^{-2} day^{-1} between MGPP and GDMP.

Significantly better results are achieved by MODIS and SMAP products than by GDMP when compared to EC GPP estimates. The ε parameterization for both MODIS and SMAP products relies on land cover type through the use of a BPLUT that defines, among others, the different ε_{max} values per land cover (Heinsch et al., 2006). In this case, the ε_{max} values ranged from 0.68 g MJ^{-1} for crops to 1.16 g MJ^{-1} for evergreen broadleaf forest. The lowest errors are observed for the SMAP product at De-Tha site (RMSD = 2.2 g m^{-2} day^{-1}), which may be partially explained by the smoother profile resulting from a gap filling method described in Section 3.1. The lowest error shown by the MODIS product for the FI-Hyy site (RMSD = 1.1 g m^{-2} day^{-1}) is a direct consequence of the poor quality data reduction performed in the pre-processing stage (described in Section 4.2.1).

At grasslands and savanna sites (SN-Dhr and ZA-Kru) in Africa, larger disagreements with EC GPP approximations are observed during the periods of growth, particularly at SN-Dhr since no water scarceness is expected due to foreseeable rainy periods. As it was reported by Martínez et al. (2018a), high EC GPP values are observed in SN-Dhr as compared to other semi-arid sites; the reason for these values may be justified, among others, by the concurrence of moderately dense herbaceous vegetation, high soil nutrient presence and grazing practices (Tagesson et al., 2016b; Martínez et al., 2018a). Regardless of the differences, the MGPP product shows one of the lowest discrepancies (RMSE = 1.7 g m^{-2} day^{-1}; MAE = 0.9 g m^{-2} day^{-1}; MBE = –0.8 g m^{-2} day^{-1}) with the EC GPP estimates along with the GDMP product (RMSE = 1.6 g m^{-2} day^{-1}; MAE = 0.9 g m^{-2} day^{-1}; MBE = –0.7 g m^{-2} day^{-1}). The low agreement with the EC GPP may be justified by two factors, the wrong ε_{max} assignment of the MGPP product (i.e. an ε_{max} belonging to croplands is assigned in the MGPP due to the land cover classification used) along with the contribution of the f_{APAR}, which is also able to account for changes in the vegetation canopy due to water stress. A direct consequence in the f_{APAR} due to water stress may be the plant photosynthesis reduction due to a less chlorophyll production (Gamon et al., 1995; Moreno et al., 2014).

Hence, a biome-specific parameterization requires accurate information on the land cover type. At global scale, a land cover map will always contain a fraction of falsely classified pixels. Quaife et al. (2008) reported an error in GPP estimated from satellite data up to 16% due to land cover misclassification. In our case, an overall accuracy around a 69% was stated globally for GLC2000 (Mayaux et al., 2006). Thus, updated versions of this information should be revised and considered on a regular basis to provide a more reliable and consistent MGPP product.

(iii) Temporal and spatial coverage

When the EO-based GPP products are compared, dissimilarities in the observations may be observed due to differences in the temporal sampling interval and data availability, which could be hindered by low quality data mostly due to cloudy conditions. For MGPP, the largest differences with other EO-based GPP products are observed at higher latitudes (Fig. 8) owing to lower MGPP performance (e.g. low incoming PAR and snow presence, see Figs. 3 and 4), and over densely forest areas (e.g. equatorial regions) due to the high presence of clouds. Although the decrease of GPP due to cloud occurrence is mainly expected by the reduction of the PAR, the GPP values could be also constrained by the accuracy of other inputs under these conditions, such as the f_{APAR}. Thus, high f_{APAR} errors (> 0.2) and low-quality inputs were taken into account in the filtering process of the MGPP product. As a result, the 10-day GPP composite is provided for every pixel when a minimum of three daily GPP estimates are available rather than for the MODIS LAI/FPAR (MOD15) product where at least one day of quality LAI/FPAR data is considered for any given 8-day period (Heinsch et al., 2003). This may result in a higher efficiency of the MODIS GPP product at cloudy areas such as the tropics where it is possible to find no cloud-free 10- or 8-day periods. These areas are easily localized in the MGPP and MODIS images for July and October over the west region of Africa and correspond mainly to the 6% of pixels labelled as bad quality (Figs. 3 and 4).

Despite of MODIS product includes suboptimal retrievals with backup solution, a relaxed constrain for the 8-day composite (i.e. only a minimum of one observation is required) and post-processing filtering method (Zhao et al., 2005), the MODIS profiles are noisy and present unexpected temporal drops at some validation sites, maybe caused by f_{APAR} diminution due to cloud conditions (see FI-Hyy and DE-Tha). As a contrast, the SMAP product shows a smoother profile resulting from a gap filling method based on the replacement of those low confidence f_{APAR} values retrieved from a long-term f_{APAR} record (Kimball et al., 2016). This method provides the advantage of a smooth and gap-free

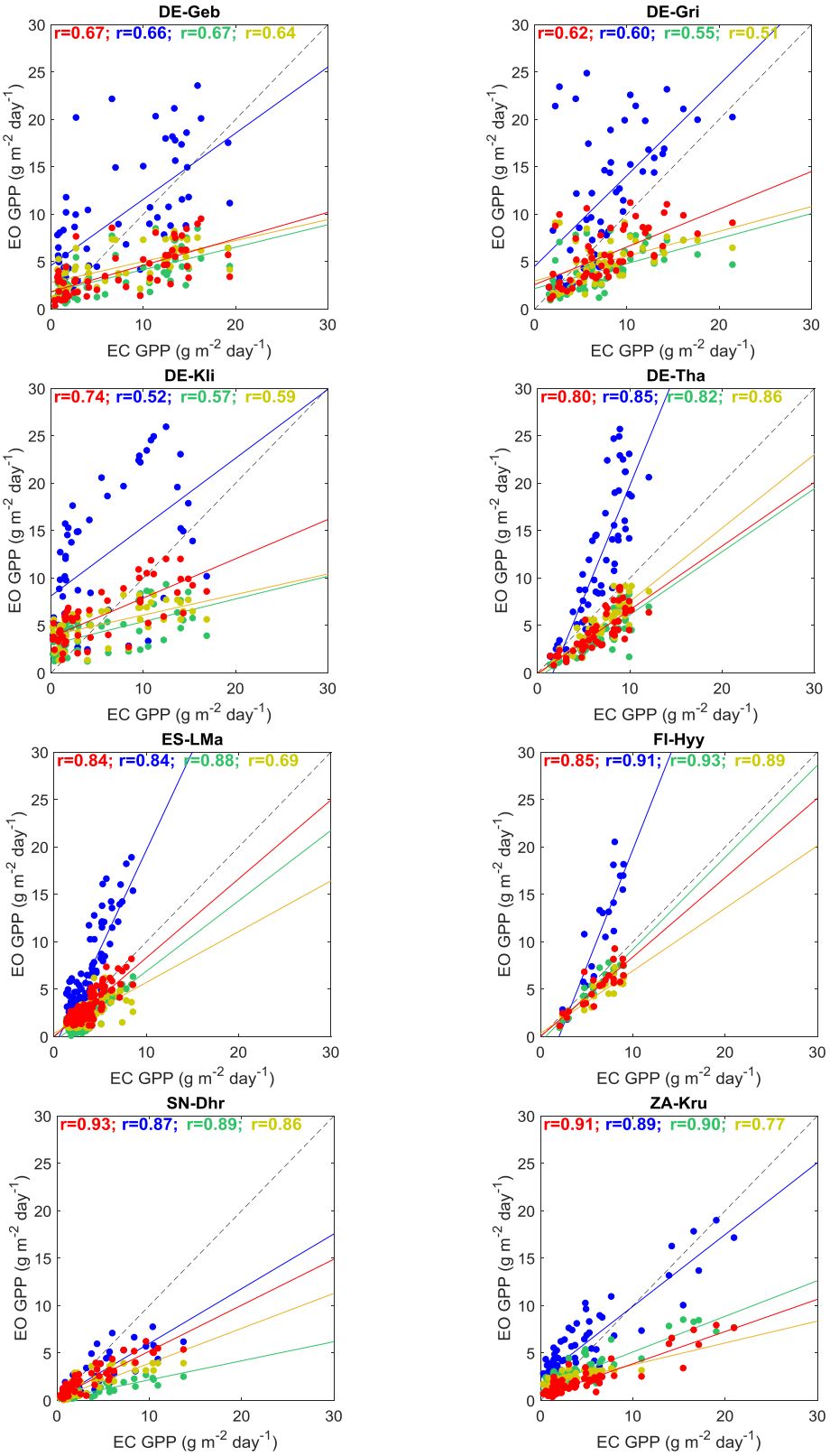

Fig. 6. Scatter plots of the different EO-based products (y-axis) *vs.* the EC tower GPP estimates for the different sites. MGPP (red dots), MODIS (green dots), GDMP (blue dots) and SMAP (yellow dots). The coefficient of correlation (*r*) is also included. (For interpretation of the references to colour in this figure legend, the reader is referred to the web version of this article.)

GPP time series as opposed to MODIS (see Fig. 4) while may reduce model accuracy to periodic and long-term climate variability, influence of current climate tendencies and severe phenomena or new land cover and land use changes (Kimball et al., 2016).

The GDMP product uses the operational 10-day CGLS f_{APAR} product at 1 km from the MARSOP project (Weiss et al., 2010). In the CGLS

f_{APAR} product persistent cloud cover artefacts are eliminated by a smoothing procedure, which confers the f_{APAR} times series with fewer missing data and a higher accuracy series when validated with EC tower GPP estimates (CGLOPS1, 2018b). Conversely, the GDMP product hardly presents gaps offering a more continuous data record (see Figs. 3 and 4).

(iv) Spatial mismatch with EC tower footprint

Generally, special attention is recommended when estimates between tower estimates and EO-based products are compared at 1-km pixel spatial resolution (Baldocchi, 2008; Zhou et al, 2016) due to the spatial representativeness of the tower, which strongly depends on local conditions like the tower's footprint (also including wind direction), soil properties, precipitation, elevation, etc. This makes more difficult to generalize tower specific parameterization into broad categories like land cover, which might also bring more uncertainties in the ε_{max} assignment.

The comparison is made at MSG/SEVIRI spatial resolution except for products with an original coarser spatial resolution such as the SMAP product. Tower flux footprints are subsamples of the MSG pixel and, thus, a worst adjustment among the EC footprint and the EO-based products can lead to differences in the GPP comparison mostly in croplands such as DE-Geb and DE-Kli. This mismatch might partially explain the differences in the magnitude for the MGPP, MODIS and GDMP products over the growing season as well as the minimum EC GPP value at the harvest not account for any of the EO-based products (at the end of the summer).

7. Conclusions

This study aimed to describe a newly launched 10-day GPP satellite product (MGPP) using SEVIRI/MSG data as part of the EUMETSAT application ground segment. The release of this newly product along with the availability of long vegetation time series LSA-SAF record (2004-present) may offer an opportunity for a better knowledge of the different ecosystem processes and terrestrial carbon modeling over the MSG disk, similarly to other missions (e.g. MODIS and Copernicus).

The skills of this new product have been assessed. In practice, one of the key issues in the successful application of this product is its simplicity in computation and robustness (i.e. low time computation and high stability) because of the use of an ensemble of LSA-SAF products as inputs (i.e. DMET, METREF, DIDSSF and MDFAPAR). Important aspects such as general global patterns and seasonal dynamics have been

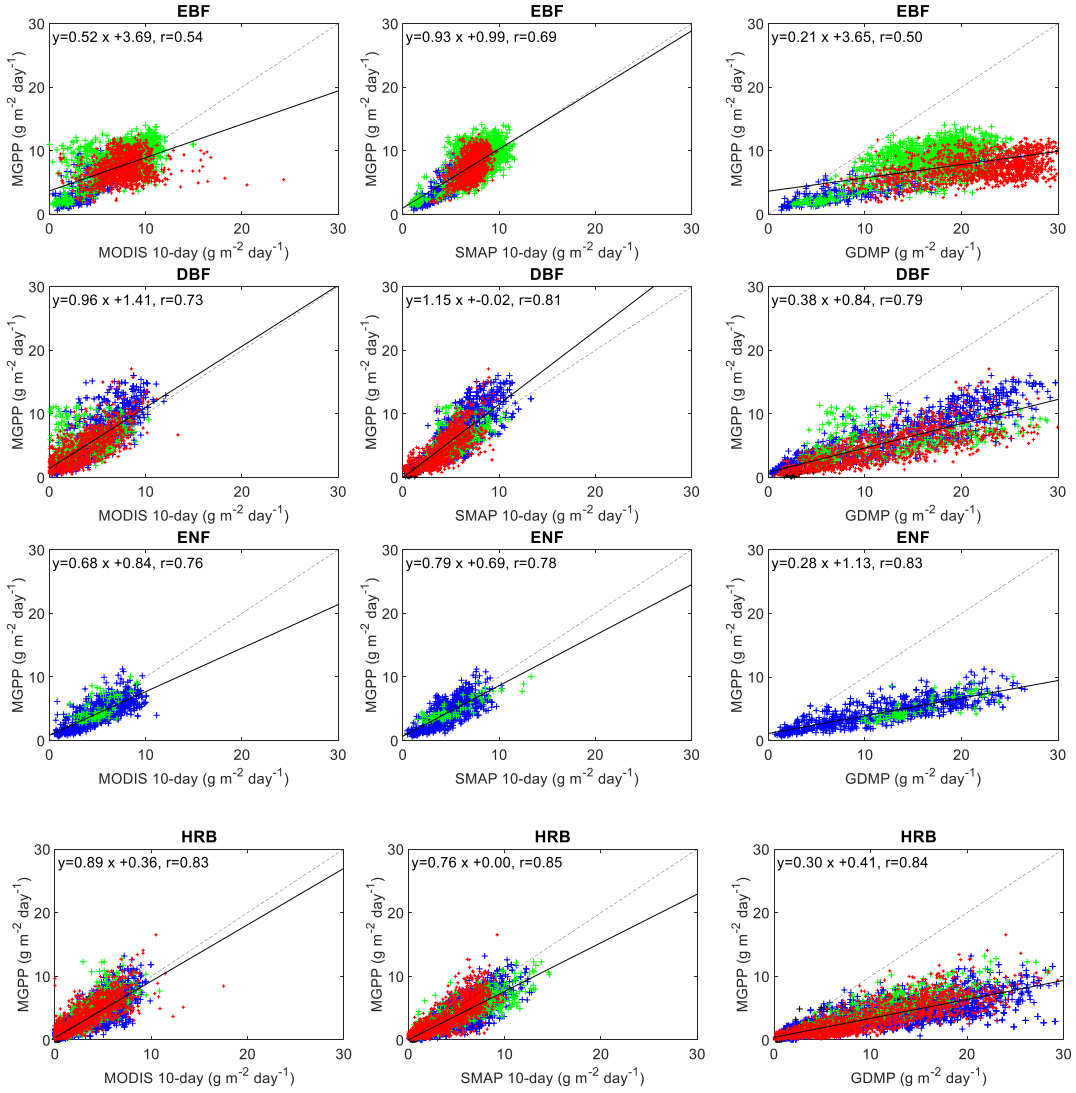

Fig. 7. MGPP product *vs.* MODIS (left), GDMP (center) and SMAP (right) products at 10-day temporal resolution (x-axis) over the MSGVAL sites for 2015–2017 regrouped in vegetation types (rows). Color code: locations over Europe (blue), Asia (black), Africa (red) and South America (green). (For interpretation of the references to colour in this figure legend, the reader is referred to the web version of this article.)

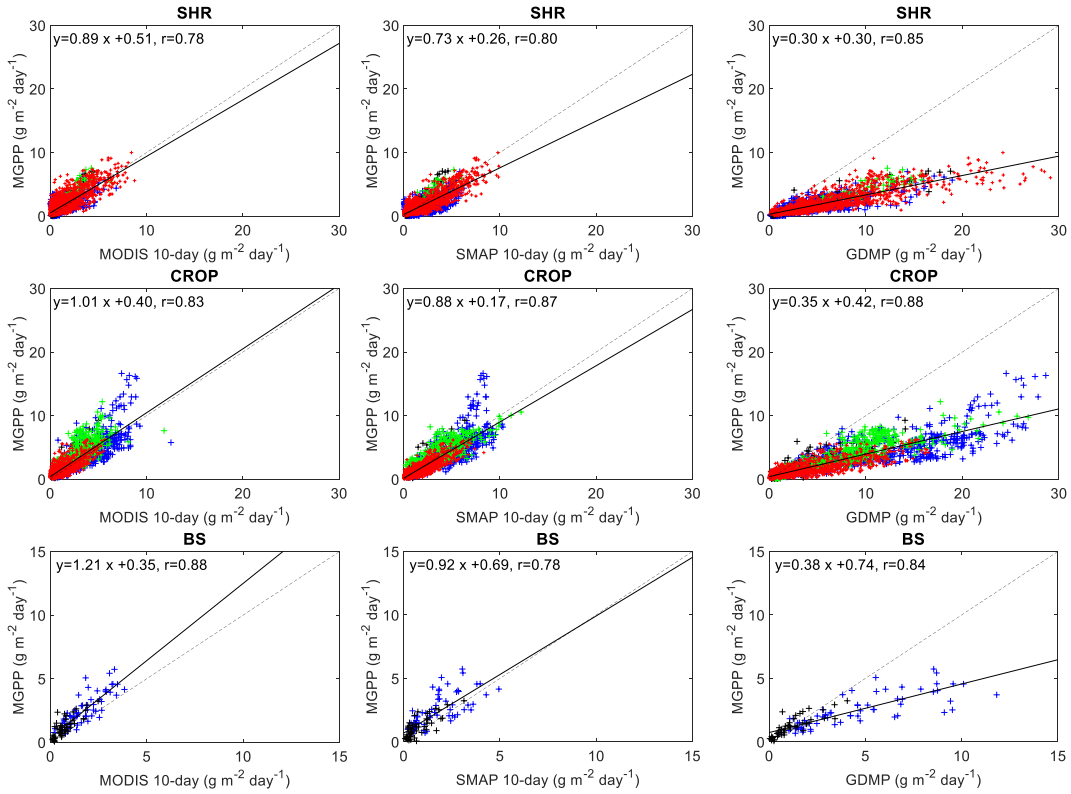

Fig. 7. (*continued*)

Table 3
Results from the assessment performed between MGPP and the three EO-based GPP products in the MSGVAL sites. MBD, MAD and RMSD are given in g m^{-2} day^{-1} for the land covers, EBF, DBF, ENF, HRB, SHR, CROP and BS. The correlation (r) between the products is also included.

Land cover	EO-based GPP product	MBD	MAD	RMSD	r
EBF	MODIS	0.3	1.9	2.5	0.54
	SMAP	0.5	1.5	1.9	0.69
	GDMP	−11.0	11.0	12.2	0.50
DBF	MODIS	1.2	1.8	2.6	0.73
	SMAP	0.7	1.6	2.1	0.81
	GDMP	−6.6	6.7	8.2	0.79
ENF	MODIS	−0.8	1.4	1.7	0.76
	SMAP	−0.3	1.1	1.4	0.78
	GDMP	−7.5	7.5	8.8	0.83
HRB	MODIS	0.1	0.9	1.3	0.83
	SMAP	−0.9	1.2	1.6	0.85
	GDMP	−5.5	5.5	7.2	0.84
SHR	MODIS	0.3	0.8	1.1	0.78
	SMAP	−0.4	0.9	1.1	0.80
	GDMP	−3.5	3.6	4.9	0.85
CROP	MODIS	0.4	0.9	1.3	0.83
	SMAP	−0.1	0.8	1.2	0.87
	GDMP	−2.7	2.9	4.6	0.88
BS	MODIS	0.6	0.7	0.9	0.88
	SMAP	0.6	0.8	1.1	0.78
	GDMP	−1.2	1.3	2.1	0.84

Note: Correlations demonstrated a significance level up to 95%.

evaluated in addition to a quantitative assessment of product performance and accuracy. Although the proposed validation exercise is constrained by the field data availability, the results have indicated the effectiveness of algorithm to provide a high confidence product to be released to the users and to be used for terrestrial ecosystems applications or production processes.

The important strengths of the MGPP product, such as the daily basis of an intermediate GPP product (MDGPP), produced internally in the LSA-SAF system, and the ability to recognize the productivity diminution due to water scarcity by means of the water stress coefficient (C_{ws}) can be of great importance for a variety of related issues. For example, the inclusion of this coefficient should benefit in the analysis of how ecosystems cope with extreme and recurrent droughts (Maselli et al., 2009; Gilabert et al., 2015; Martínez et al., 2018a), particularly over central Africa due to the MSG's nominal position at 0° longitude and wide area frequent observations in this area. Nevertheless, this scheme is not always sufficient and several areas of research have been identified as possible improvements for future implementations for the MGPP algorithm and output.

The quality of the MGPP product can be hampered by several factors, such as the high presence of clouds and snow during the 10-day period, particularly over the tropics or high latitudes in Europe. As an improvement, a gap filling and filtering of the daily f_{APAR} time series can be performed as it was proposed in Martínez et al. (2018a). Unfortunately, this temporal filling can only be accomplished if an entire year of the daily f_{APAR} MSG product is available, limiting the near-real time of MGPP distribution. Other potential cause that may strongly influence the MGPP performance refers to the effect of low temperature values and the variability of the ε_{max} found within individual biomes and its dependence with the chosen land cover. Improvements may be led to update the individual values within biomes whenever a better quality of land cover maps or new information via on going ecosystem research become available. Future work is expected to assess the feasibility of including the thermal effect in the MGPP product.

Acknowledgments

This study was assisted by the Land Surface Analysis SAF (EUMETSAT) and ESCENARIOS project from the Ministerio de Ciencias, Innovación y Universidades of Spain (CGL2016-75239-R) co-funded by FEDER. Dr. Tagesson was funded by SNSB (Dnr 95/16). Thanks are

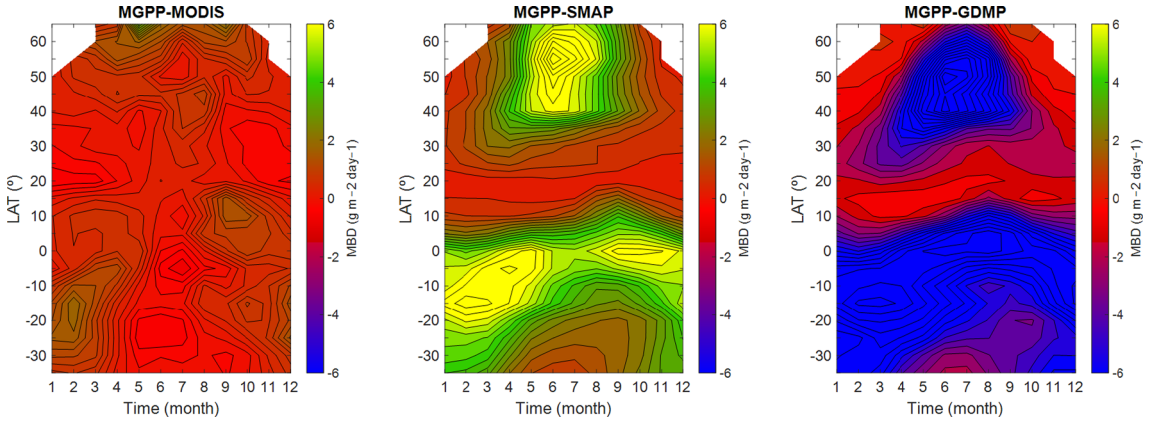

Fig. 8. Differences of the mean GPP values among MGPP, MODIS, GDMP and SMAP GPP products. The differences are computed at every 10°-latitude bands in each month during the period 2015–2017.

given to the NASA EOSDIS Land Processes to Distributed Active Archive Center (LP DAAC) at the USGS/Earth Resources Observation and Science (EROS) Center for the MOD17A2 data distribution, to NASA DAAC at the National Snow and Ice Data Center Distributed Active Archive Center (NSIDC) for the SMAP (SPL4CMDL) data and to the EU Copernicus Global Land Service programme for GDMP data. Special thanks are given to the anonymous reviewers for their valuable suggestions.

Appendix A. . MDGPP performance against EC tower GPP estimates

As a benchmark to better understand the quality and reliability of the 10-day MSG GPP product (MGPP), an assessment between the interim daily MSG GPP product (MDGPP) and the EC tower GPP estimates was performed at daily temporal scale.

The results (Table A.1) exhibit slightly higher errors and lower correlations that those found at 10-day scale (Table 2), mainly explained by the noise attributed to the daily temporal variability. In some cases, the obtained errors were still below those errors observed for the EO-based products at 10-day scale (e.g. DE-Gri, De-Kli, ES-LMa, and Za-Kru).

The number of observations (percent value) with a residual between MDGPP and EC GPP estimates falling below the optimal (< 1.0 g m^{-2} day^{-1}), target (< 2.0 g m^{-2} day^{-1}) and threshold (< 3.0 g m^{-2} day^{-1}) values were also computed. Very similar percentages were obtained (i.e. 45%, 65% and 75% for optimal, target and threshold accuracies, respectively) as compared with those obtained at 10-day scale (see Section 5.4), confirming a high consistency between both MDGPP and MGPP products.

Table A1
Results derived from the comparison between MDGPP and EC tower GPP estimates, at daily temporal scale. RMSE, MBE and MAE are written in g m^{-2} day^{-1}. The correlation between the MDGPP and the EC GPP estimates is also shown.

Site	MBE	MAE	RMSE	r
DE-Geb	−3.7	4.5	6.0	0.67
DE-Gri	−1.7	3.3	4.4	0.52
DE-Kli	0.6	3.2	4.0	0.67
DE-Tha	−2.2	2.6	3.1	0.68
ES-LMa	−0.6	1.1	1.4	0.77
FI-Hyy	−0.7	1.5	1.8	0.82
SN-Dhr	−0.8	1.0	1.8	0.86
ZA-Kru	−2.4	2.6	4.2	0.87

Appendix B. . Explanatory power analysis for the MGPP product

As a further analysis of the MGPP product understanding, a statistical test was carried out to quantify which factors (i.e. incident photosynthetically active radiation, vegetation state and water stress) control the gross primary production. For this purpose, the explanatory power of the used Monteith light use efficiency approach (Eq. (1)) was analyzed considering different inputs (Gilabert et al., 2015). The correlation between MGPP and the product of its inputs (PAR, f_{APAR} and C_{ws}) sequentially added is computed. Firstly, the contribution of the PAR (r_{PAR}) is assessed by computing the Pearson's correlation coefficient (r) between MGPP and ε_{max} PAR (Eq. (B.1)). Secondly, the contribution of f_{APAR} ($r_{f_{APAR}}$) is calculated by subtracting r_{PAR} from the correlation between MGPP and $\varepsilon_{max} f_{APAR}$ PAR (Eq. (B.2)). Finally, the contribution of the C_{ws} ($r_{C_{ws}}$) is assessed by subtracting r_{PAR} and $r_{f_{APAR}}$ from 1 (Eq. (B.3)).

$$r_{PAR} = r(\text{MGPP}, \varepsilon_{max}\,\text{PAR}) \tag{B.1}$$

$$r_{f_{APAR}} = r(\text{MGPP}, \varepsilon_{max} f_{APAR}\,\text{PAR}) - r_{PAR} \tag{B.2}$$

$$r_{C_{ws}} = 1 - r_{PAR} - r_{f_{APAR}} \tag{B.3}$$

The spatial pattern of the contributions of the inputs in the MGPP model is described in Fig. B.1 by means of the Hovmoller diagrams. The mean values of each correlation (r_{PAR}, $r_{f_{APAR}}$, and $r_{C_{ws}}$) against latitude is computed for each month of the study period. Fig. B.1. reveals the PAR as the most

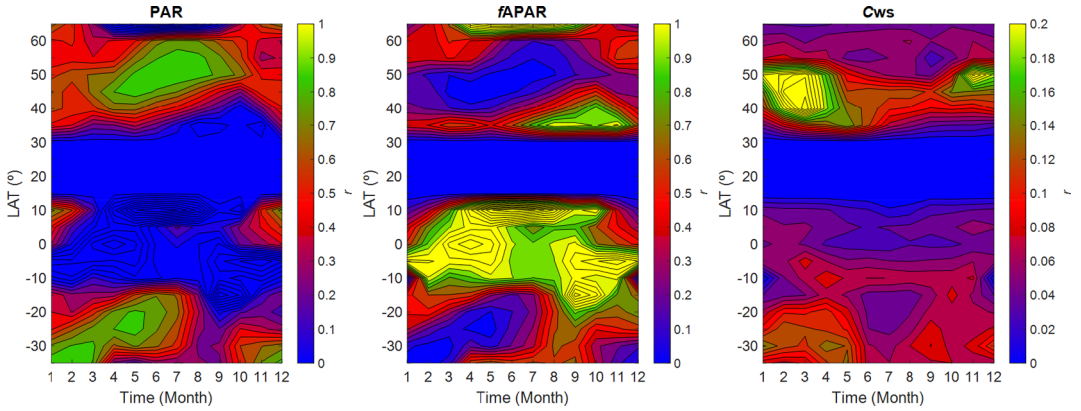

Fig. B1. Hovmoller diagrams of the contribution of each of the MGPP inputs by computing the incremental correlation between MGPP and its inputs sequentially added. Monthly values against latitude during the 2015–2017 period.

influential variable at high latitudes in the North and South hemisphere during the summer season (where the PAR shows greater inter-annual variability). In these regions the PAR justifies around 60% of the MGPP variance ($r > 0.8$), which is complemented by almost 40% of the variance explained by the f_{APAR} ($r \cong 0.2$). As was reported by Gilabert et al. (2015), this connection between the PAR and f_{APAR} deals with the strong correlation between both variables observed for many types of vegetation. However, the f_{APAR} highlights its contribution when both PAR and f_{APAR} are decoupled (Gilabert et al., 2015). This lack of connection arises, for example, when the maximum of both vegetation and solar cycles are not reached at the same time, such as in the equatorial regions. In these areas, $r_{f_{APAR}}$ shows the highest values for almost all the year, maybe explained by the low solar cycle variations due to the high solar irradiance along the entire year. The contributions from C_{ws} is almost an order of magnitude lower than that of f_{APAR} and highest values are observed on high latitudes at periods of the year where the water availability is reduced (green and yellow colors).

References

Allen, R.G., Pereira, L.S., Raes, D., Smith, M., 1998. Crop Evapotranspiration: Guide-lines for Computing Crop Water Requirements. In: Irrigation and Drainage Paper No. 56. FAO, Rome, Italy, pp. 300.

Anthoni, P.M., Knohl, A., Rebmann, C., Freibauer, A., Mund, M., Ziegler, W., et al., 2014. Forest and agricultural land-use-dependent CO2 exchange in Thuringia, Germany. Global Change Biol. 10 (12), 2005–2019.

Archibald, S.A., Kirton, A., van der Merwe, M.R., Scholes, R.J., Williams, C.A., Hanan, N., 2009. Drivers of inter-annual variability in net ecosystem exchange in a semi-arid savanna ecosystem, South Africa. Biogeosciences 6 (2), 251–266.

Bahtaa, Y.T., Jordaanb, A., Muyambob, F., 2016. Communal farmers' perception of drought in South Africa: policy implication for drought risk reduction. Int. J. Disaster Risk Reduct. 20, 39–50.

Baldocchi, D.D., 2008. Breathing' of the terrestrial biosphere: lessons learned from a global network of carbon dioxide flux measurements systems. Aust. J. Bot. 56, 1–26.

Bartholomé, E., Belward, A.S., 2005. GLC2000: a new approach to global land cover mapping from Earth observation data. Int. J. Remote Sens. 26 (9), 1959–1977.

Bojinski, S., Verstraete, M., Peterson, T.C., Richter, C., Simmons, A., Zemp, M., 2014. The concept of essential climate variables in support of climate research, applications, and policy. Am. Meterorol. Soc. 95 (9), 1431–1443.

Casals, P., Lopez-Sangil, L., Carrara, A., Gimeno, C., Nogués, S., 2011. Autotrophic and heterotrophic contributions to short-term soil CO2 efflux following simulated summer precipitation pulses in a Mediterranean dehesa. Global Biogeochem. Cycles 25 (GB3012), 1–12.

CGLOPS1, 2018a. Copernicus Global Land Operations "Vegetation and Energy" Product User Manual for Dry Matter Productivity (DMP) and Gross Dry Matter Productivity (GDMP). Collection 1 km, version 2- CGLOPS1_PUM_DMP1km-V2, February 2018, 47 pp.

CGLOPS1, 2018b. Copernicus Global Land Operations "Vegetation and Energy" Algorithm Theorical Basis document (ATBD) for Dry Matter Productivity (DMP) and Gross Dry Matter Productivity (GDMP). Collection 1 km, version 2- CGLOPS1_ATBD_DMPV2, February 2018, 53 pp.

GTOS, 2010. Implementation plan for the global observing system for climate in support of the UNFCCC (2010 update). GCOS Rep. 138, 186 pp. (Available online at www.wmo.int/pages/prog/gcos/Publications/gcos-138.pdf).

Camacho, F., García-Haro, F.J., Sánchez-Zapero, J., Fuster, B., 2017. Validation Report MSG/SEVIRI Vegetation Parameters (VEGA). SAF/LAND/UV/VR_VEGA_MSG, Issue 3.1. (available on-line at landsaf.meteo.pt).

Congalton, R.G., Gu, J., Yadav, K., Thenkabail, P., Ozdogan, M., 2014. Global land cover mapping: a review and uncertainty analysis. Rem. Sens. 6, 12070–12093.

Connolly, J., Roulet, N.T., Seaquist, J.W., Holden, N.M., Lafleur, P.M., Humphreys, E.R., et al., 2009. Using MODIS derived fPAR with ground based flux tower measurements to derive the light use efficiency for two Canadian peatlands. Biogeosciences 6, 225–234.

De Almeida, C.T., Coll, R., Sores, L., de Oliveira, L.E., Ramos, M.C., 2018. Improvements of the MODIS gross primary productivity model based on a comprehensive uncertainty assessment over the Brazilian Amazonia. ISPRS J. Photogramm. Rem. Sens. 145 (Part B), 268–283.

De Bruin, H.A.R., Trigo, I.F., Bosveld, F.C., Meirink, J.F., 2016. A thermodynamically based model for actual evapotranspiration of an extensive grass field close to FAO reference, suitable for remote sensing application. J. Hydrometeorol. 17, 1373–1382.

Di Gregorio, A., Jansen, L.J., 2000. Land Cover Classification System (LCCS): Classification Concepts and User Manual. Rome, Italy, Food and Agriculture Organization of the United Nations.

Fernandes, R., Plummer, S.E., Nightingale, et al., 2014. Global Leaf Area Index Product Validation Good Practices. CEOS Working Group on Calibration and Validation - Land Product Validation Sub-Group. Version 2.0. https://doi.org/10.5067/doc/ceoswgcv/lpv/lai.002.

Fuster, B., Sánchez-Zapero, J., Camacho, F., García-Haro, F.J., Campos-Taberner, M., 2017. Validation of the Climate Data Record of EUMETSAT LSA SAF SEVIRI/MSG LAI, FAPAR and FVC products. Proceedings of the V RAQRS conference, Torrent, September 2017. (in press).

Gamon, J.A., Field, C.B., Goulden, M.L., Griffin, K.L., Hartley, A.E., Joel, G., Peñuelas, J., Valentini, R., 1995. Relationships between NDVI, canopy structure, and photosynthesis in three californian vegetation types. Ecol. Appl. 5, 28–41.

Garbulsky, M.F., Penuelas, J., Papale, D., Ardo, J., Goulden, M.L., Kiely, G., et al., 2010. Patterns and controls of the variability of radiation use efficiency and primary productivity across terrestrial ecosystems. Glob. Ecol. Biogeogr. 19, 253–267.

García-Haro, F.J., Camacho, F., 2016. Algorithm Theoretical Basis Document for Vegetation parameters (VEGA), LSA-421 (MDFVC), LSA-422 (MTFVC), LSA-423 (MDLAI), LSA- 424 (MTLAI), LSA-425 (MDFAPAR), LSA-426 (MTFAPAR), LSA-450 (MTFVCR), LSA- 451 (MTLAI-R), LSA-452 (MTFAPAR-R). SAF/LAND/UV/VR_VEGA/2.0. Available on-line at. http://landsaf.meteo.pt.

García-Haro, F.J., Campos-Taberner, M., Muñoz-Marí, J., Laparra, V., Camacho, F., Sánchez-Zapero, J., Camps-Valls, G., 2018. Derivation of global vegetation biophysical parameters from EUMETSAT polar system. ISPRS J. Photogramm. Remote Sens. 139, 57–74.

Geiger, B., Meurey, C., Lajas, D., Franchistéguy, L., Carrer, D., Roujean, J.-L., 2008. Near real time provision of downwelling shortwave radiation estimates derived from satellite observations. Meteorol. Appl. 15, 411–420.

Gilabert, M.A., Moreno, A., Maselli, F., Martínez, B., Chiesi, M., Sánchez-Ruiz, S., et al., 2015. Daily GPP estimates in Mediterranean ecosystems by combining remote sensing and meteorological data. ISPRS J. Photogramm. Remote Sens. 102, 184–197.

Gilabert, M.A., Sánchez-Ruiz, S., Moreno, A., 2017. Annual gross primary production from vegetation indices: a theoretically sound approach. Rem. Sens. 9, 193.

Gitelson, A., Gamon, J., 2015. The need for a common basis for defining light-use efficiency: implications for productivity estimation. Remote Sens. Environ. 156, 196–201.

Gitelson, A., Peng, Y., Arkebauer, T.J., Schepers, J., 2014. Relationships between gross primary production, green LAI, and canopy chlorophyll content in maize: implications for remote sensing of primary production. Remote Sens. Environ. 144, 65–72.

Heinsch, F.A., Reeves, M., Votava, P., Kang, S., Milesi, C., Zhao, M., et al., 2003. User's guide: GPP and NPP (MOD17A2/A3) products. NASA MODIS land algorithm, version 2.0 1–57.

Heinsch, F.A., Maosheng, Z., Running, S.W., Kimball, J.S., Nemani, R.R., Davis, K.J., et al., 2006. Evaluation of remote sensing based terrestrial productivity from MODIS using regional tower eddy flux network observations. IEEE Trans. Geosci. Rem. Sens. 44 (7), 1908–1925.
Hussain, M.Z., Grünwald, T., Tenhunen, J.D., Li, Y.L., Mirzae, H., Bernhofer, C., et al., 2011. Summer drought influence on CO2 and water fluxes of extensively managed grassland in Germany. Agric. Ecosyst. Environ. 141, 67–76.
Iqbal, M., 1983. An Introduction to Solar Radiation. Academic Press, Toronto, pp. 390.
Jones, L.A., Kimball, J.S., Reichle, R.H., Madani, N., Glassy, J., Ardizzone, J.V., et al., 2017. The SMAP level 4 carbon product for monitoring ecosystem land-atmosphere CO2 exchange. IEEE Trans. Geosci. Remote Sens. 55 (11), 6517–6532.
Kang, Y., Kan, S., Ma, X., 2009. Climate change impacts on crop yield, crop water productivity and food security – a review. Prog. Nat. Sci. 19 (12), 1665–1674.
Kimball, J.S., Jones, L.A., Zhang, K., Heinsch, F.A., McDonald, K.C., Oechel, W.C., 2009. A satellite approach to estimate land-atmosphere CO_2 exchange for boreal and arctic biomes using MODIS and AMSR-E. IEEE Trans. Geosci. Remote Sens. 47 (2), 569–587.
Kimball, J.S., Jones, L.A., Glassy, J.P., Reichle, R., 2014. SMAP Algorithm Theoretical Basis Document, Release A: L4 Carbon Product. SMAP Project, JPL D-66484, Jet Propulsion Laboratory, Pasadena CA. 76 pp. (271_L4_C_RevA_web.pdf, 2.7 MB).
Kimball, J.S., Jones, L.A., Glassy, J., Stavros, E.N., Madani, N., Reichle, R.H., et al., 2016. Soil Moisture Active Passive Mission L4_C Data Product Assessment (Version 2 Validated Release). GMAO Office Note No. 13 (Version 1.0), 37 pp, NASA Goddard Space Flight Center, Greenbelt, MD, USA. Available from http://gmao.gsfc.nasa.gov/pubs/office_notes.
Kimball, J.S., Jones, L.A., Glassy, J., Reichle, R., 2017. SMAP L4 Global Daily 9 km Carbon Net Ecosystem Exchange, Version 3. NASA National Snow and Ice Data Center Distributed Active Archive Center, Boulder, Colorado USA 10.5067/O4HAQJEWWUU8.
Lasslop, G., Reichstein, M., Papale, D., Richardson, A., Arneth, A., Barr, A., et al., 2010. Separation of net ecosystem exchange into assimilation and respiration using a light response curve approach: critical issues and global evaluation. Glob. Change Biol. 16, 187–208.
LSA SAF, 2012. Algorithm Theoretical Basis Document (ATBD) for Down-Welling Surface Shortwave Flux (DSSF). SAF/LAND/MF/ATBD_DSSF/1.0. Available on-line at http://landsaf.meteo.pt.
Madani, N., Kimball, J.S., Affleck, D.L.R., Kattge, J., Graham, J., van Bodegom, P.M., et al., 2014. Improving ecosystem productivity modeling through spatially explicit estimation of optimal light use efficiency. J. Geophys. Res. Biogeosci. 119, 1755–1769.
Martínez, B., Camacho, F., Verger, A., García-Haro, F.J., Gilabert, M.A., 2013. Intercomparison and quality assessment of MERIS: MODIS and SEVIRI FAPAR products over the Iberian Peninsula. Int. J. Appl. Earth Obs. Geoinf. 21, 463–476.
Maselli, F., Papale, D., Puletti, N., Chirici, G., Corona, P., 2009. Combining remote sensing and ancillary data to monitor the gross productivity of water-limited forest ecosystems. Remote Sens. Environ. 113, 657–667.
Martínez, B., Sánchez-Ruiz, S., Gilabert, M.A., Moreno, A., Taberner, M.C., García-Haro, F.J., et al., 2018a. Retrieval of daily gross primary production over Europe and Africa from an ensemble of SEVIRI/MSG products. Int. J. Appl. Earth Obs. Geoinf. 65, 124–136.
Martínez, B., Sánchez-Ruiz, S., Campos-Taberner, M., García-Haro, F.J., Gilabert, M.A., 2018b. Algorithm Theoretical Basis Document for Gross Primary Production (GPP). SAF/LAND/UV/ATBD_GPP/1.4. Available on-line at. http://landsaf.meteo.pt.
Martínez, B., Sánchez-Ruiz, S., Campos-Taberner, M., García-Haro, F.J., Gilabert, M.A., 2018c. Validation Report Document for Gross Primary Production. SAF/LAND/UV/VR_MGPP/v1.3. Available on-line at. http://landsaf.meteo.pt.
Mayaux, P., Eva, H., Gallego, J., Strahler, A.H., Herold, M., Agrawal, S., et al., 2006. Validation of the global land cover 2000 map. IEEE Trans. Geosci. Remote Sens. 44 (7), 1728–1739.
Metz, B., Davidson, O., Coninck, H.D., Loos, M., Meyer, L., 2006. Special Report of the Intergovernmental Panel on Climate Change. Intergovernmental Panel on Clim. Change, World Meterorol. Organ, Geneva.
Monson, R., Baldocchi, D., 2014. Terrestrial biosphere-atmosphere fluxes. Cambridge University Press.
Monteith, J.L., 1972. Solar radiation and productivity in tropical ecosystems. J. Appl. Ecol. 9, 747–766.
Moreno, A., Gilabert, M.A., Camacho, F., Martínez, B., 2013. Validation of daily global solar irradiation images from MSG over Spain. Renew. Energy J. 60, 332–342.
Moreno, A., Maselli, F., Chiesi, M., Genesio, L., Vaccari, F., Seufert, G., Gilabert, M.A., 2014. Monitoring water stress in Mediterranean semi-natural vegetation with satellite and meteorological data. Int. J. Appl. Earth Observ. 26, 246–255.
Nemani, R.R., Keeling, C.C., Hashimoto, H., Jolly, W.M., Piper, S.C., Tucker, C.J., 2003. Climate-driven increases in global terrestrial net primary production from 1982 to 1999. Science 300, 1560–1563.
Potter, C.S., Klooster, S., Myneni, R., Genovese, V., Tan, P.N., Kumar, V., 2003. Continental-scale comparisons of terrestrial carbon sinks estimated from satellite data and ecosystem modeling 1982–1998. Global Planet. Change 39, 201–213.
Preschet, A.-K., Grünwald, T., Bernhofer, C., 2010. Land use regulates carbon budgets in eastern Germany: from NEE to NBP. Agric. For. Meteorol. 150, 1016–1025.
Quaife, T., Quegan, S., Disney, M., Lewis, P., Lomas, M., Woodward, F.I., 2008. Impact of land cover uncertainties on estimates of biospheric carbon fluxes. Global Biogeochem. Cycles 22, GB4016.
Roujean, J.L., Leroy, M., Dechamps, P.Y., 1992. A bidirectional reflectance model of the earth's surface for the correction of remote sensing data. J. Geophys. Res. 97, 455–468.
Roujean, J.L., Bréon, F.M., 1995. Estimating PAR absorbed by vegetation from bidirectional reflectance measurements. Remote Sens. Environ. 51, 373–384.
Running, S., Nemani, R., Heinscgm, F., Zhao, M., Reeves, M., Hashimoto, H., 2004. A continuous satellite-derived measure of global terrestrial primary production. Bioscience 54 (6), 547–560.
Running, S.W., Zhao, M., 2015. Daily GPP and Annual NPP (MOD17A2/A3) Products NASA Earth Observing System MODIS Land Algorithm. Useŕs Guide. Version 3.0 For Collection 6.
Sánchez-Ruiz, S., Moreno, A., Piles, M., Maselli, F., Carrara, A., Running, S., Gilabert, M.A., 2017. Quantifying water stress effect on daily light use efficiency in Mediterranean ecosystems using satellite data. Int. J. Digital Earth 10 (6), 623–638.
Schaefer, K., Schwalm, C.R., Williams, C., Arain, M.A., Barr, A., Chen, J.M., et al., 2012. A model-data comparison of gross primary productivity: results from the North American Carbon Program site synthesis. J. Geophys. Res. 117, G03010. https://doi.org/10.1029/2012JG001960.
Schmidt, W., 1915. Strahlung und Verdunstung an freien Wasserflächen; ein Beitrag zum Warmehaushalt des Weltmeers und zum Wasserhaushalt der Erde (Radiation and evaporation over open water surfaces; a contribution to the heat budget of the world ocean and to the water budget of the earth). Annalen der Hygrographie und Maritimen Meteorologie 43 (111–124), 169–178.
Suni, T., Rinne, J., Reissell, A., Altimir, N., Keronen, P., Rannik, Ü., et al., 2003. Long-term measurements of surface fluxes above a Scots pine forest in Hyytiäla southern Finland, 1996–2001. Boreal Environ. Res. 8, 287–301.
Tagesson, T., Fensholt, R., Guiro, I., Rasmussen, M.O., Huber, S., Mbow, C., et al., 2015a. Ecosystem properties of semiarid savanna grassland in West Africa and its relationship with environmental variability. Glob. Change Biol. 21 (1), 250–264.
Tagesson, T., Fensholt, R., Cropley, F., Guiro, I., Horion, S., Ehammer, A., Ardö, J., 2015b. Dynamics in carbon exchange fluxes for a grazed semi-arid savanna ecosystem in West Africa. Agric. Ecosyst. Environ. 205, 15–24.
Tagesson, T., Ardö, J., Gurio, I., Cropley, F., Mbow, C., Horion, S., et al., 2016a. Very high CO2 exchange fluxes at the peak of the rainy season in a West African grazed semi-arid savanna ecosystem. Danish J. Geograp. 116, 93–109.
Tagesson, T., Fensholt, R., Cappelaere, B., Mougin, E., Horion, S., Kergoat, L., et al., 2016b. Spatiotemporal variability in carbon exchange fluxes across the Sahel. Agric. Forest Meteorol. 226–227, 108–118.
Trigo, I.F., et al., 2011. The satellite application facility on land surface analysis. Int. J. Remote Sens. 32, 2725–2744. https://doi.org/10.1080/01431161003743199.
Tsalyuk, M., Kelly, M., Getz, W.M., 2017. Improving the prediction of African savanna vegetation variables using time series of MODIS products. ISPRS J. Photogramm. Remote Sens. 131, 77–91.
Tramontana, G., Jung, M., Schwalm, C.R., Ichii, K., Camps-Valls, G., Radulu, B., et al., 2016. Predicting carbon dioxide and energy fluxes across global FLUXNET sites with regression. Biogeosciences 13, 4291–4313.
Trigo, I., de Bruin, H., 2016. Algorithm Theoretical Basis Document for Reference Evapotranspiration (DMETREF) PRODUCTS: LSA-303 (DMETREF). LAND/IPMA/ATBD_METREF/1.1. Available on-line at. http://landsaf.meteo.pt.
Turner, D.P., Gower, S.T., Cohen, W.B., Gregory, M., Maiersperger, T.K., 2002. Effects of spatial variability in light use efficiency on satellite-based NPP monitoring. Remote Sens. Environ. 80 (3), 397–405.
Vicca, S., Balzarolo, M., Filella, I., Granier, A., Herbst, M., Knohl, A., et al., 2016. Remotely-sensed detection of effects of extreme droughts on gross primary production. Sci. Rep. 6, 28269.
Zhang, Y., Yu, G., Yang, J., Wimberly, M.C., Zhang, X., Tao, J., et al., 2014. Climate-driven global changes in carbon use efficiency. Global Ecol. Biogeography, (Global Ecol. Biogeogr.) 23, 144–155.
Zhao, M., Heinsch, F.A., Nemani, R.R., Running, S.W., 2005. Improvements of the MODIS terrestrial gross and net primary production global data set. Remote Sens. Environ. 95 (2), 164–175.
Zhao, M., Running, S.W., 2010. Drought-induced reduction in global terrestrial net primary production from 2000 through 2009. Science 329, 940–943.
Zhao, M., Running, S.W., Heinsch, F.A., Nemani, R.R., 2011. MODIS derived terrestrial primary production. Land Remote Sensing and Global Environmental Change. Springer, New York, pp. 635–660.
Zhou, Y., Wu, X., Ju, W., Chen, J.M., Wang, S., Wang, H., et al., 2016. Global parameterization and validation of a two-leaf light use efficiency model for predicting gross primary production across FLUXNET sites. J. Geophys. Res.: Biogeosci. 121, 1045–1072.
Waring, H.R., Running, S.W., 2007. Forest ecosystems, 3rd ed. Academic Press, San Diego, CA.
Weiss, M., Baret, F., Eerens, H., Swinnen, E., 2010. fAPAR over Europe for the past 28 years: A temporally consistent product derived from AVHRR and VEGETATION Sensors. Proc. 3rd International symposium "Recent Advances in Quantitative Remote Sensing", Valencia, Spain, 27/9-1/10 2010.
Weiss, M., Baret, F., Block, T., Koetz, B., Burini, A., Scholze, B., et al., 2014. On line validation exercise (OLIVE): A web based service for the validation of medium resolution land products. Application to FAPAR products. Remote Sensing 6, 4190–4216.
Yi, Y., Kimball, J.S., Jones, L.A., Reichle, R.H., Nemani, R., Margolis, H.A., 2013. Recent climate and fire disturbance impacts on boreal and arctic ecosystem productivity estimated using a satellite-based terrestrial carbon flux model. J. Geophys. Res.: Biogeosci. 118, 1–17.
Yuan, W., Liu, S., Zhou, G., Zhou, G., Tieszen, L.L., Baldocchi, D., et al., 2007. Deriving a light use efficiency model from eddy covariance flux data for predicting daily gross primary production across biomes. Agric. For. Meteorol. 143 (3–4), 189–207.